Post-phagocytosis activation of NLRP3 inflammasome by two novel T6SS effectors

Hadar Cohen[1], Noam Baram[1], Chaya M. Fridman[1], Liat Edry-Botzer[1], Dor Salomon[1]* and Motti Gerlic[1]*

[1]Department of Clinical Microbiology and Immunology, Sackler Faculty of Medicine, Tel Aviv University, Tel Aviv 6997801, Israel.

Lead Contact: Motti Gerlic PhD, Department of Clinical Microbiology and Immunology, Sackler Faculty of Medicine, Tel Aviv University, Tel Aviv 69978, Israel. Tel. (Office): +972-3-640-9400, Fax: +972-3-640-9160, e-mail: mgerlic@tauex.tau.ac.il

*Corresponding authors: Dor Salomon PhD (D.S) and Motti Gerlic (M.G) PhD, Department of Clinical Microbiology and Immunology, Sackler Faculty of Medicine, Tel Aviv University, Tel Aviv 69978, Israel. Tel. (Office): +972-3-640-7636, e-mails: dorsalomon@mail.tau.ac.il, mgerlic@tauex.tau.ac.il; ORCID: https://orcid.org/0000-0002-2009-9453 and https://orcid.org/0000-0001-9518-1833, respectively.

Summary

The type VI secretion system (T6SS) is used by bacteria to deliver toxic effectors directly into target cells. Most T6SSs mediate antibacterial activities, whereas the potential anti-eukaryotic role of T6SS remains understudied. Here, we found a *Vibrio* T6SS that delivers two novel effectors into mammalian host immune cells. We showed that these effectors induce a pyroptotic cell death in a phagocytosis-dependent manner; we identified the NLRP3 inflammasome as being the underlying mechanism leading to the T6SS-induced pyroptosis. Moreover, we identified a compensatory T6SS-induced pathway that is activated upon inhibition of the canonical pyroptosis pathway. Genetic analyses revealed possible horizontal spread of this T6SS and its anti-eukaryotic effectors into emerging pathogens in the marine environment. Our findings reveal novel T6SS effectors that activate the host inflammasome and possibly contribute to virulence and to the emergence of bacterial pathogens.

Keywords

T6SS, Vibrio, Secretion system, cell death, pyroptosis, IL-1β, Caspase-1, Gasdermin, GSDMD, GSDME.

Introduction

Innate immune responses combat infections but may also drive pathological inflammation. The innate immune system engages an array of pattern-recognition receptors (PRR) that are expressed by cells found at the defensive front line against infections, including macrophages, dendritic cells, neutrophils, and others. PRRs can detect a variety of microbial determinants termed pathogen-associated molecular patterns (PAMPs). Moreover, damaged host cells can also trigger PRRs by releasing danger-associated molecular patterns (DAMPs) (Wallach et al., 2014; Wen et al., 2013).

Some PRRs of the innate immune system are assembled into a high-molecular weight complex called “the inflammasome” after sensing DAMPs or PAMPs. Inflammasome complexes are considered central components of innate immunity because of their ability to kill an infected cell (a cell death process that is termed pyroptosis), or by their activation and the subsequent secretion of mature pro-inflammatory cytokines interleukin 1β (IL-1β) and IL-18 (Lamkanfi and Dixit, 2014; Schroder and Tschopp, 2010) Inflammasomes can be divided into: (1) a canonical pathway in which Caspase-1 is cleaved into a catalytically active enzyme, and (2) non-canonical pathways in which Caspase-11 is activated (Lamkanfi and Dixit, 2014). The canonical inflammasome comprises one of the nucleotide-binding oligomerization domain (NOD), leucine-rich repeat (LRR)-containing protein (NLR) family members, including NLRP1, NLRP3, NLRC4 or the DNA sensor absent in melanoma 2 (AIM2), all of which contain either a pyrin domain (PYD) or a caspase recruitment domain (CARD) (Schroder and Tschopp, 2010). These domains interact with apoptosis-associated speck-like protein (ASC), leading to its polymerization into large helical filaments known as ASC specks by facilitating self-interactions of the

PYD of ASC (Franklin et al., 2014; Proell et al., 2013). The CARD domain of the ASC specks recruits Caspase-1 via a CARD-CARD interaction, leading to Caspase-1 clustering that permits autocleavage and formation of the active Caspase-1 p10/p20 tetramer (Lamkanfi and Dixit, 2014). Activated Caspase-1 processes pro-IL-1β and pro-IL-18 into their mature forms. Simultaneously, activated Caspase-1 cleaves gasdermin D (GSDMD) into a C-terminal fragment (GSDMD-CT) and N-terminal fragment (GSDMD-NT) (Liu et al., 2016; Shi et al., 2015). GSDMD-NT oligomerizes in membranes to form pores which promote IL-1β release and pyroptotic cell death (Lieberman et al., 2019; Liu et al., 2016).

The type VI secretion system (T6SS) is a widespread macromolecular protein secretion apparatus that translocates proteins into neighboring cells in a contact-dependent manner (Bingle et al., 2008; Boyer et al., 2009; Mougous et al., 2006; Pukatzki et al., 2006). Most of the T6SS-secreted proteins are toxic effectors capable of manipulating target cells. Although many T6SS effectors are antibacterial toxins, some T6SSs deliver effectors with anti-eukaryotic activities into host cells, thus promoting virulence or defense against predation (Monjarás Feria and Valvano, 2020). Nevertheless, the anti-eukaryotic potential of T6SSs remains understudied and possibly underappreciated (Dar et al., 2018; Hachani et al., 2016).

T6SS is common in vibrios (Dar et al., 2018), a genus of Gram-negative marine bacteria that includes many established and emerging human pathogens (e.g. *Vibrio cholerae, Vibrio parhaemolyticus,* and *Vibrio vulnificus*), which are a leading cause of gastroenteritis and wound infections (Baker-Austin et al., 2018). Vibrios preferentially grow in warm (>15°C) marine environments; remarkably, the rise in sea surface temperatures correlates with the spread of vibrios and with *Vibrio*-associated human illness (Roux et al., 2015; Vezzulli et al., 2016).

Vibrio proteolyticus (*V. proteolyticus*) is a Gram-negative marine bacterium that was isolated from diseased corals (Cervino et al., 2008); it was also shown to cause mortality in fish (Bowden et al., 2018) and in the crustacean model organism, *Artemia* (Verschuere et al., 2000). *V. proteolyticus* does not possess a type III secretion system (T3SS) that can mediate delivery of effector proteins directly into host cells (Miller et al., 2019; Ray et al., 2016). Nevertheless, it encodes a secreted pore-forming hemolysin (Cohen et al., 2020; Ray et al., 2016) and three different T6SSs (T6SS1-3) (Ray et al., 2016, 2017). T6SS1 mediates both antibacterial and anti-eukaryotic activities, whereas T6SS3 does not play any role in bacterial competition and its hypothesized anti-eukaryotic potential remains to be investigated (Ray et al., 2017).

In a recent study in which we investigated the secreted *V. proteolyticus* cytotoxic hemolysin, VPRH, we observed the existence of another, VPRH-independent cell death that occurred only during infections of primary macrophages, but not in the cultured cell lines HeLa or RAW264.7 (Cohen et al., 2020). Thus, in this study, we set out to determine whether *V. proteolyticus* T6SSs can lead to cell death in primary macrophages, and if so, to decipher the underlying mechanism. We found that *V. proteolyticus* T6SS3, but not T6SS1, induced a phagocytosis-dependent cell death in bone marrow-derived macrophages (BMDMs). Using chemical and genetics approaches, we identified pyroptosis as the underlying mechanism of T6SS3-induced cell death, and specifically the NLRP3 inflammasome. Moreover, we found that a pathway comprising gasdermin E (GSDME) and caspase-3 compensates for GSDMD absence in response to T6SS3 activity, in a NLRP3-dependent manner. Lastly, we identified a new T6SS3 activator and two novel T6SS3 anti-eukaryotic effectors that are needed to induce inflammasome-mediated

115 cell death in BMDMs. Overall, our findings shed new light on the interplay between
116 T6SS, phagocytosis and the NLRP3 inflammasome, and underscore the virulence
117 potential of T6SSs.
118
119 **Results**
120
121 ***T6SS3 induces cell death in primary macrophages***
122 We previously showed that *V. proteolyticus* induces two types of cell death in
123 BMDMs: (1) a rapid cell death that is mediated by the pore-forming hemolysin,
124 VPRH, and (2) a slower cell death that is VPRH-independent (Cohen et al., 2020).
125 The underlying mechanism driving the latter remains unknown. *V. proteolyticus*
126 harbors three T6SSs (T6SS1-3). We hypothesized that one or more of these T6SSs
127 are responsible for the observed VPRH-independent cell death. Previously, we
128 showed that T6SS1 mediates interbacterial competition and manipulates the actin
129 cytoskeleton in macrophages (Ray et al., 2017). We also proposed that T6SS3
130 targets eukaryotic cells (Ray et al., 2017). Furthermore, we reported that T6SS1 and
131 T6SS3 are functional under laboratory conditions; however, we did not detect any
132 T6SS2 activating conditions (Ray et al., 2017). Therefore, we excluded T6SS2 from
133 subsequent analyses, and we focused on a possible contribution of T6SS1 and
134 T6SS3 to cell death in BMDMs.
135 To investigate the role of T6SS1 and T6SS3 in cell death, we first sought to
136 further induce T6SS activity. We reasoned that if a T6SS is responsible for inducing
137 cell death, then hyper-activating it would improve our ability to monitor the cell death
138 phenotype by (1) maximizing its amplitude, (2) shortening the time to onset, and (3)
139 allowing us to lower the multiplicity of infection (MOI). We previously reported that H-

NS, the histone-like nucleoid-structuring protein, is a negative regulator of T6SSs in vibrios and that its deletion results in hyper-activation of T6SS (Salomon et al., 2014, 2015) . Thus, we generated a *V. proteolyticus* strain with a deletion in a gene we named *hns1* (*VPR01S_RS04360*); it encodes an H-NS that is very similar to VP1133, the previously studied H-NS protein from *V. parahaemolyticus* (Salomon et al., 2014). Importantly, the deletion was performed in a Δ*vprh* background to allow the subsequent monitoring of VPRH-independent cell death. We then determined the effect of *hns1* deletion on T6SS1 and T6SS3 activity. To this end, we monitored the expression and secretion of VgrG1 and Hcp3, hallmark secreted tail tube components of T6SS1 and T6SS3, respectively. We found that *hns1* deletion resulted in elevated secretion of both VgrG1 and Hcp3, compared to their secretion from the parental Δ*vprh* strain (**Figure 1a**). Notably, the secretion of VgrG1 and Hcp3 was T6SS1- and T6SS3-dependent, respectively, as evident from their absence in the supernatant fractions of strains deleted for *tssG1* (T6SS1^{-}) and *tssL3* (T6SS3^{-}), which are core structural genes required for the activity of T6SS1 and T6SS3, respectively. These results indicate that *hns1* deletion de-represses T6SS1 and T6SS3, leading to their constitutive activation and thus elevated secretion.

Next, we used real-time microscopy (IncucyteZOOM) to monitor VPRH-independent cell death kinetics in BMDMs. Whereas infection with the Δ*vprh* strain resulted in negligible cell death three hours post infection, the Δ*vprh*/Δ*hns1* mutant induced a rapid cell death in which ~80% of the cells in the culture were dead within this time frame (set as 100% Normalized Area Under the Curve (AUC); **Figure 1b,c**). Remarkably, the rapid cell death evident in the Δ*vprh*/Δ*hns1* mutant was completely abrogated upon genetic inactivation of T6SS3 (Δ*vprh*/Δ*hns1*/T6SS3^{-}), but not upon genetic inactivation of T6SS1 (Δ*vprh*/Δ*hns1*/T6SS1^{-}) (**Figure 1b,c**). Notably, genetic

165 inactivation of T6SS1 or T6SS3 had no significant effect on growth during the
166 relevant time frame compared to the parental Δ*vprh*/Δ*hns1* strain in either MLB or
167 DMEM media (**Figure 1d**), nor did it affect bacterial swimming motility (**Figure 1e**).
168 Taken together, these results suggest that T6SS3, but not T6SS1, mediates a
169 VPRH-independent cell death in BMDMs.

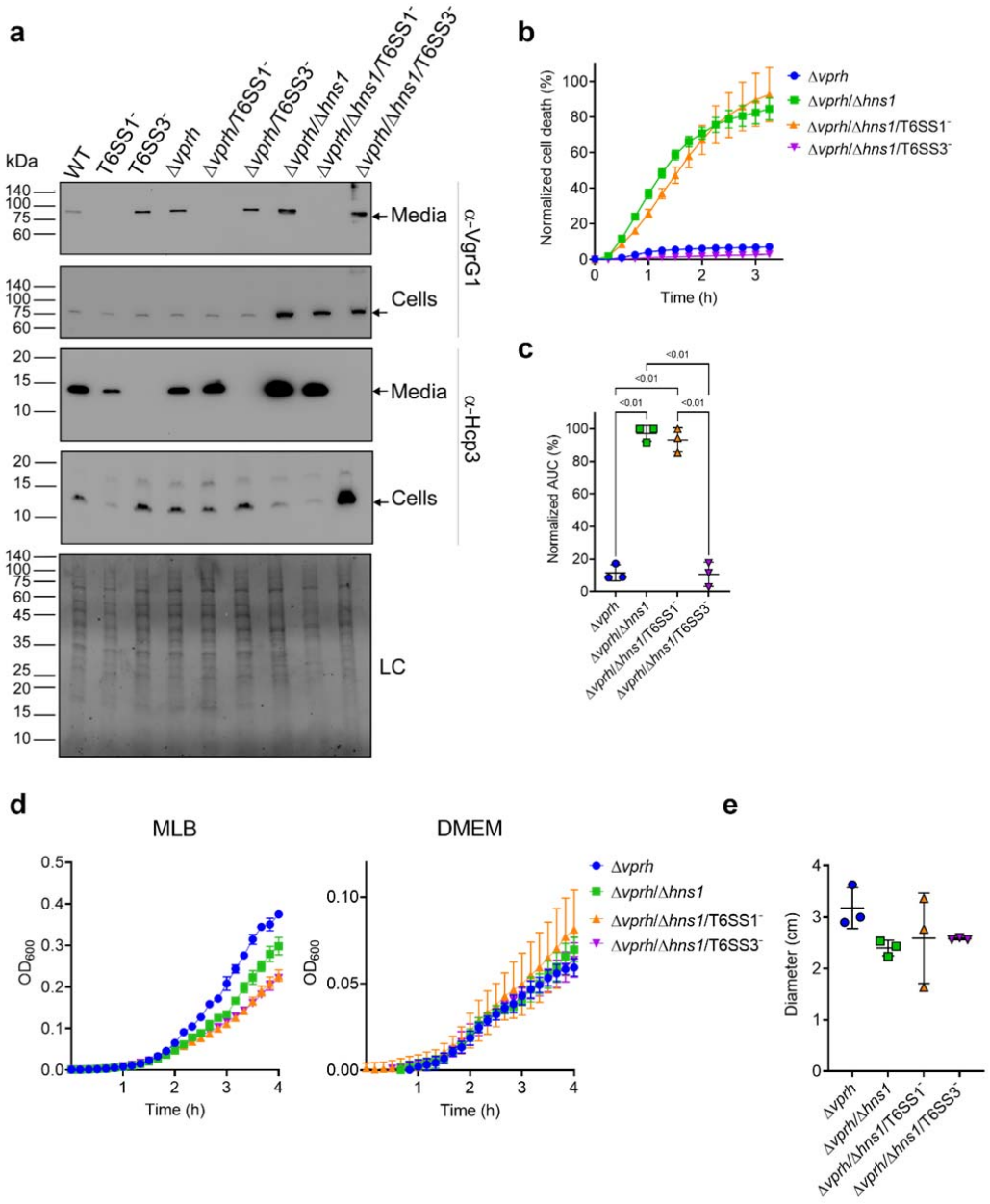

170

Figure 1: *T6SS3 induces cell death in primary macrophages*

(a) Expression (cells) and secretion (media) of Hcp3 and VgrG1 from the indicated *V. proteolyticus* strains were detected by immunoblotting using specific antibodies against Hcp3 and VgrG1, respectively. Loading control (LC) is shown for total protein lysate. **Arrows denote the expected band size. (b-c)** Assessment of cell death upon infection of BMDMs *with V. proteolyticus* strains. Approximately $3.5*10^4$ BMDMs were seeded into 96-well plates in triplicate and were primed with LPS (100 ng/mL) 3 hours prior to infection with *V. proteolyticus* strains at MOI 5. Propidium iodide (PI) was added to the medium prior to infection, and its kinetic uptake was assessed using real-time microscopy (IncucyteZOOM) (b) and then analyzed as the area under the curve (AUC) of the percentage of PI-positive cells normalized to the number of cells in the wells (c). **(d)** Growth of *V. proteolyticus* strains, used in (b), in MLB or DMEM media at 30°C or 37°C, respectively, measured as absorbance at 600 nm (OD_{600}). **(e)** Swimming motility of *V. proteolyticus* strains used in (b), measured as migration of a soft-agar plate after overnight incubation at 30°C. The data in (a, b, d) are a representative experiment out of 3 independent experiments. The data in (c) and (e) are the combined results of 3 independent experiments presented as the mean ± SD. In (c) and (e), statistical comparisons between the different *V. proteolyticus* strains were performed using a one-way ANOVA, followed by Tukey's multiple comparison test. Significant *P* values (<0.05) are denoted above.

T6SS3 induces pyroptotic cell death in BMDMs

We previously demonstrated that a VPRH-independent cell death is observed upon infection of BMDMs, but not in HeLa cells or RAW 264.7 macrophages (Cohen et al., 2020). Unlike the two cell lines, BMDMs contain a functional cell death mechanism known as pyroptosis (Cohen et al., 2020; Proell et al., 2013). Pyroptosis is a form of necrotic and inflammatory regulated cell death induced by the inflammasome complex. Assembly of the inflammasome leads the maturation and secretion of pro-inflammatory cytokines, such as IL-1β (Man et al., 2017). Therefore, we hypothesized that inflammasome activation and pyroptosis are the mechanisms

underlying the VPRH-independent, T6SS3-dependent cell death in BMDMs. To test this hypothesis, we monitored the effect of specific inflammasome inhibitors on T6SS3-mediated cell death. Using real-time microscopy, we observed that addition of either inhibitors, MCC950 (blocks ASC oligomerization by inhibiting the canonical and non-canonical NLRP3 inflammasome (Shao et al., 2015)) or Vx765 (a potent and selective competitive inhibitor of Caspase-1 (Church et al., 2008)) resulted in delayed and reduced cell death during infection with Δ*vprh*/Δ*hns1* bacteria (~40% reduction as measured by calculating the AUC), compared with a DMSO-treated control (**Figure 2a,b**). As expected, inactivation of T6SS1 had no effect on Δ*vprh*/Δ*hns1*-induced cell death nor on the protective effect of the inhibitors, whereas inactivation of T6SS3 abrogated the cell death phenotype. These results support our hypothesis that T6SS3 induces cell death in BMDMs via an inflammasome-dependent pyroptotic pathway.

Further support for this hypothesis was obtained by monitoring the cleavage and secretion of the inflammasome-dependent cytokine, IL-1β, upon infection with *V. proteolyticus* strains. As shown in **Figure 2c-e**, IL-1β cleavage and secretion were dependent on the presence of a functional T6SS3 in Δ*vprh*/Δ*hns1* strains, and they were inhibited (**Figure 2c**) or undetected (**Figure 2d,e**) when inflammasome inhibitors were added. However, secretion of TNFα (an NF-κB-dependent, inflammasome-independent cytokine) was independent of T6SS3 activity and was unaffected by addition of inflammasome inhibitors (**Figure 2c**). Additional hallmark pyroptotic processes, such as the cleavage and release of Caspase-1 and GSDMD, were apparent upon infection of BMDMs with the Δ*vprh*/Δ*hns1* strain; however, they were undetected upon inactivation of T6SS3 or upon the addition of inflammasome

225 inhibitors (**Figure 2d,e**). Taken together, these results suggest that T6SS3 induces

226 an inflammasome-dependent, pyroptotic cell death in BMDMs

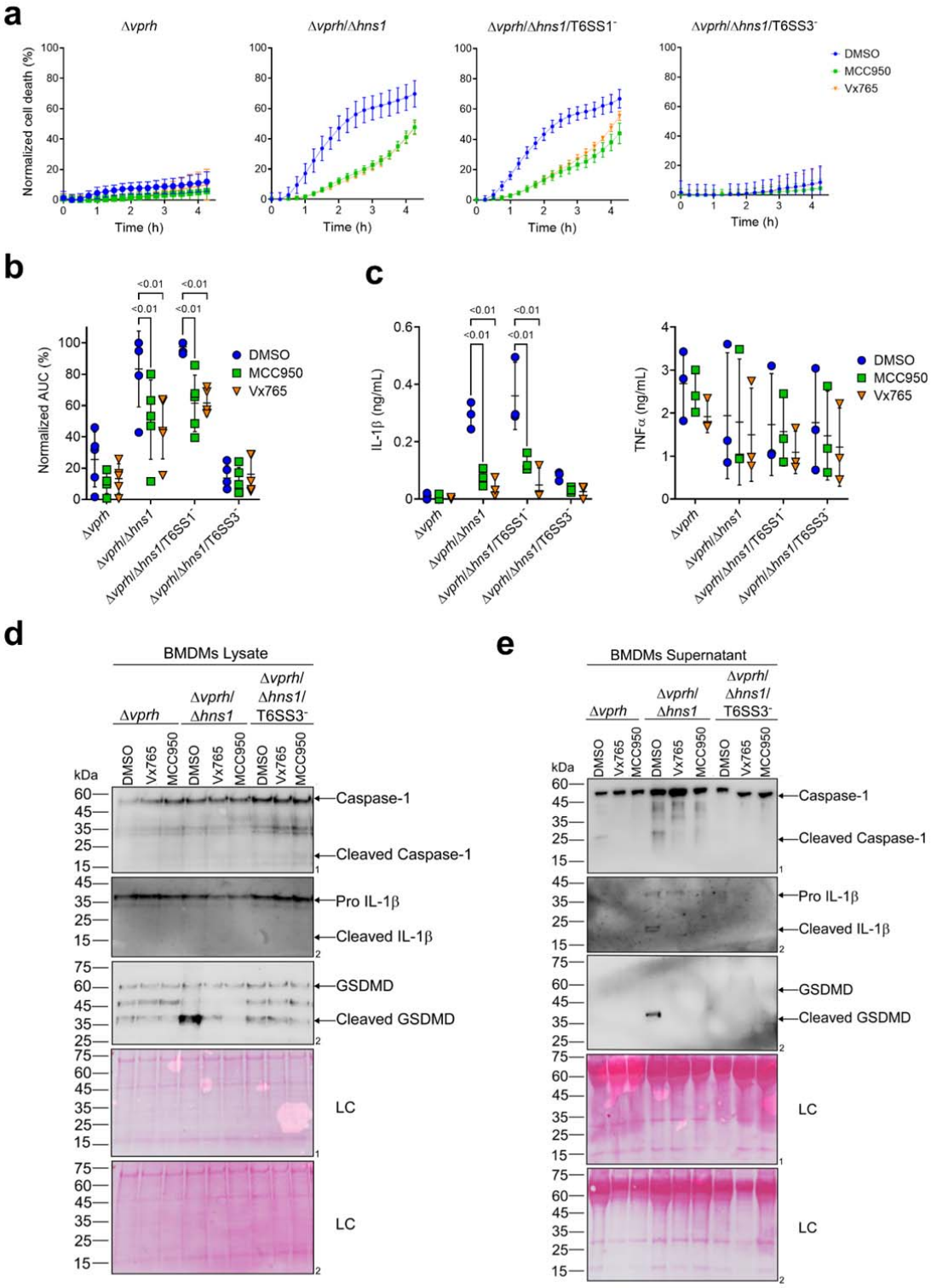

227

228 **Figure 2: T6SS3 induces pyroptotic cell death in BMDMs**

229 Approximately $3.5*10^4$ wild-type BMDMs were seeded into 96-well plates in 6

230 replicates and were primed using LPS (100 ng/mL) for 3 hours prior to infection with

V. proteolyticus strains at MOI 5. Where indicated, inflammasome inhibitors Vx765 (25 μM) or MCC950 (2 μM), with the addition of PI (1 μg/mL), were added to the cells 30 minutes prior to bacterial infection. DMSO was used as the solvent control. **(a-b)** PI kinetic uptake was assessed using real-time microscopy (IncucyteZOOM) (a) and then graphed as the AUC of the percentage of PI-positive cells normalized to the number of cells in the wells (b). **(c)** Cell supernatants from experiments described in (a) were collected 3 hours post infection. IL-1β and TNFα secretion were measured using commercial ELISA kits. **(d-e)** Caspase-1, GSDMD, and IL-1β were detected in BMDM lysate (d) and supernatant (e) by immunoblotting (the number on the right of each blot denotes the blot number). The data in (a) represent n≥3 independent experiments. Statistical comparisons in (b-c) between the different treatments were performed using RM two-way ANOVA, followed by Turkey's multiple comparison test. The results are shown as the mean ± SD of n≥3 independent experiments; significant differences (P<0.05) are denoted only for comparisons between inflammasome inhibitors of cells infected with the same bacterial strain. The results shown in (d-e) represent 2 independent experiments. Arrows denote the expected band size.

T6SS3 activates the NLRP3 inflammasome in BMDMs

Different members of the NLR family, including NLRP1 and NLRP3, can induce inflammasome assembly and activation, leading to pyroptotic cell death (Bauernfried et al., 2021; Lamkanfi and Dixit, 2014). NLRP3 is the most studied inflammasome-activating NLR; it is activated during bacterial, viral, and fungal infections, as well as in sterile inflammation mediated by endogenous DAMPs (Swanson et al., 2019). To identify the specific inflammasome pathway that is activated by T6SS3 in BMDMs, we generated BMDMs from knock-out (KO) mice in different inflammasome pathways (i.e., *Nlrp1*$^{-/-}$ and *Nlrp3*$^{-/-}$) and infected them with *V. proteolyticus* strains. Using real-time microscopy, we found that the death of BMDMs derived from NLRP1 KO mice was comparable to that of BMDMs generated from WT mice. However, infection of NLRP3 KO BMDMs resulted in delayed cell death and ~60% reduction in

the calculated AUC (**Figure 3a & Figure SF1a**). Furthermore, hallmark processes of inflammasome-mediated cell death, such as IL-1β, Caspase-1, and GSDMD cleavage and release, which were induced in a T6SS3-dependent manner, were abrogated only in *Nlrp3*$^{-/-}$ BMDMs (**Figure 3b-d**). TNFα secretion, which was used as a control, was not affected in either of the KO mouse BMDMs (**Figure 3b**), thus confirming that priming (i.e., the NF-κB-dependent pathway) remained unaffected in the *Nlrp3*$^{-/-}$ BMDMs.

NLRP3 can also be activated by the necroptotic cell death pathway, which is induced by pseudo-kinase MLKL (Conos et al., 2017; Lawlor et al., 2015). To confirm that T6SS3 directly activated the NLRP3-induced cell death rather than it being an indirect consequence of a secondary mechanism of necroptotic cell death, we also monitored cell death in *Mlkl*$^{-/-}$ BMDMs. As expected, MLKL deficiency did not affect the induction of the T6SS3-mediated cell death (**Figure 3a & Figure SF1a**) or IL-1β, Caspase-1, and GSDMD cleavage and release (**Figure 3b-d**) in BMDMs. Thus, we concluded that T6SS3 activates a pyroptotic cell death program that is mediated directly by the NLRP3 inflammasome.

To confirm that the observed NLRP3-dependent phenotypes are indeed mediated by bacterial T6SS3 activity, we complemented the deletion in *tssL3*, which was used to generate T6SS3^{-} bacterial strains, from an arabinose-inducible plasmid (pTssL3). The complementation of *tssL3* in trans restored the secretion of Hcp3 (**Figure SF1b**), as well as all of the tested inflammasome-mediated phenotypes, including cell death and IL-1β, Caspase-1, and GSDMD cleavage and release (**Figure 3e,f & Figure SF1c,d**). Importantly, TNFα secretion was not affected upon BMDMs infection with the TssL3-complemented *V. proteolyticus* strain (**Figure SF1e**). Notably, over-expression of TssL3 had no effect on bacterial growth in MLB

286 media (**Figure SF1f**), but had a minor positive effect on bacterial growth in DMEM

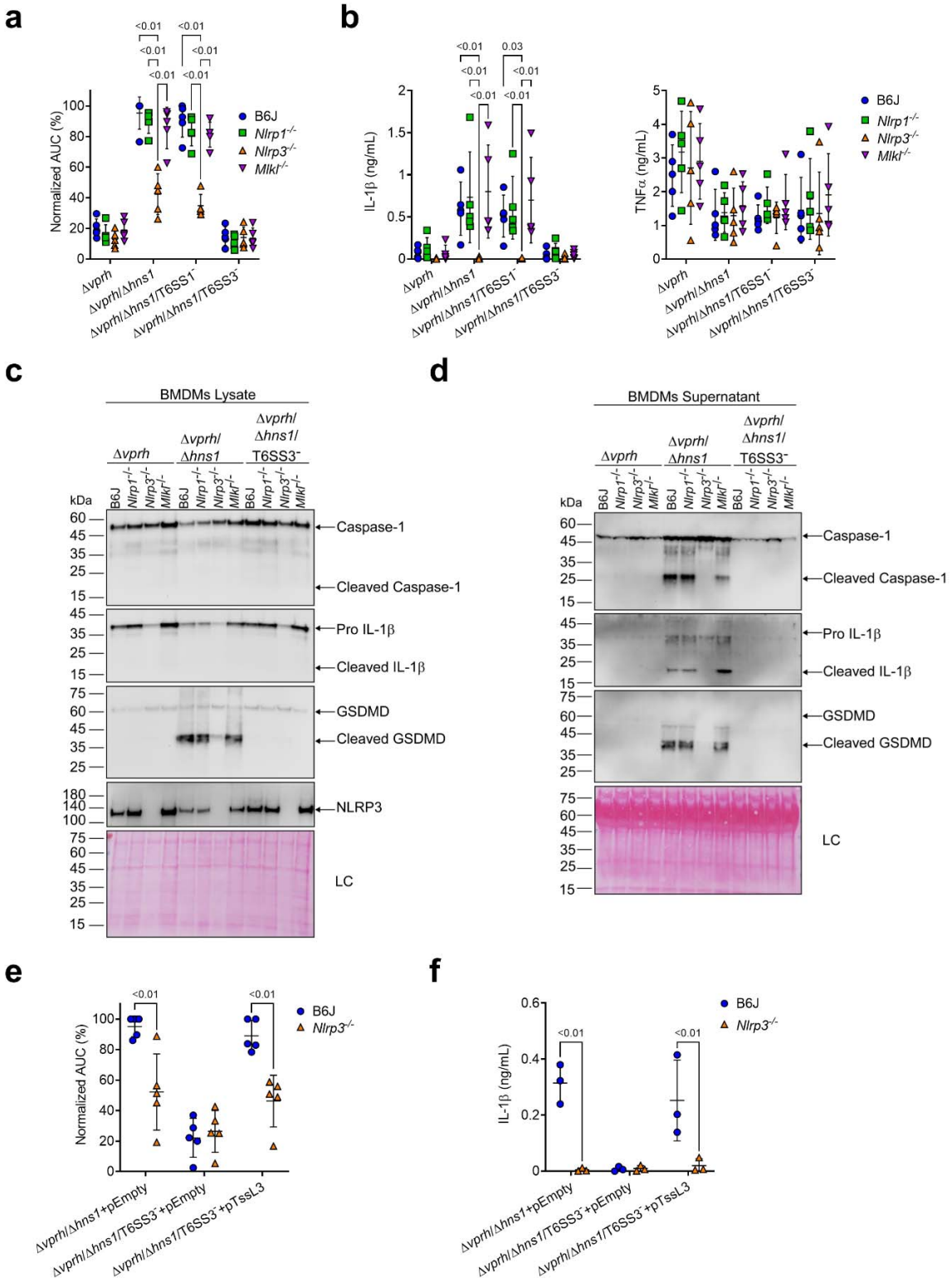

media (**Figure SF1f**).

Figure 3: T6SS3 activates the NLRP3 inflammasome in BMDMs

Approximately 3.5*10^4 wild-type (B6J), *Nlrp1*$^{-/-}$, *Nlrp3*$^{-/-}$ and *Mlkl*$^{-/-}$ BMDMs were seeded into 96-well plates in 6 replicates and were primed using LPS (100 ng/mL) for 3 hours prior to infection with *V. proteolyticus* strains at MOI 5. In (e-f), 0.05% arabinose was added to the media prior bacterial infection. **(a, e)** PI uptake was assessed using real-time microscopy (IncucyteZOOM) and then graphed as the AUC of the percentage of PI-positive cells normalized to the number of cells in the wells. **(b, f)** Cell supernatants from experiments described in (a) or (e), respectively, were collected 3 hours post infection. IL-1β and TNFα secretion were measured using commercial ELISA kits. **(c-d)** NLRP3, Caspase-1, GSDMD, and IL-1β were detected in BMDM lysate (c) and supernatant (d) by immunoblotting (the number on the right side of each blot denotes the blot number). Arrows denote the expected band size. Statistical comparisons in (a-b) and (e-f) between the different treatments were performed using RM two-way ANOVA, followed by Turkey's multiple comparison test. The results are shown as the mean ± SD of 5 independent experiments; significant differences (P<0.05) are denoted only for comparisons between mice strains infected with the same bacterial strain. The results in (c-d) represent 2 independent experiments.

GSDME partially compensates for GSDMD absence in T6SS3-induced pyroptosis and IL-1β secretion

A recent report suggested that in the absence of GSDMD, a cascade comprising Caspase-1, Caspase-8 , Caspase-3 and GSDME can lead to cell death in BMDMs (Tsuchiya et al., 2019). To investigate whether T6SS3 can induce this cascade, we monitored *Gsdmd*$^{-/-}$ BMDMs upon infection with *V. proteolyticus* strains. Using real-time microscopy, we found that in contrast with the negligible cell death observed upon infection of *Nlrp3*$^{-/-}$ BMDMs (**Figure 4a,b**), *V. proteolyticus* strains containing an active T6SS3 (i.e., Δ*vprh*/Δ*hns1* and Δ*vprh*/Δ*hns1*/T6SS1^{-}) induced a significant cell death in the absence of GSDMD, albeit delayed, compared to that observed in

BMDMs from WT mice. Remarkably, IL-1β secretion from *Gsdmd*$^{-/-}$ BMDMs infected with the Δ*vprh*/Δ*hns1* or the Δ*vprh*/Δ*hns1*/T6SS1^{-} strain was comparable to that detected in BMDMs generated from WT mice (**Figure 4c**). As before, TNFα secretion was not affected in either of the KO mouse-derived BMDMs (**Figure 4c**). Moreover, while we detected the hallmark pyroptotic phenotypes in infected BMDMs generated from WT mice (i.e., cleaved and released Caspase-1, IL-1β, and GSDMD), in *Gsdmd*$^{-/-}$ BMDMs we observed the cleavage of Caspase-3 (but not Caspase-8) and GSDME, in addition to cleavage and release of IL-1β (**Figure 4d,e**). These results suggest that in the absence of GSDMD, T6SS3 can induce a cell death cascade comprising Caspase-1, Caspase-3, and GSDME. Therefore, GSDME can compensate, at least partially, for the absence of GSDMD. Notably, activation of this alternative cascade still requires the NLRP3 inflammasome, since cleaved Caspase-3 and GSDME were absent in *Nlrp3*$^{-/-}$-derived BMDMs infected with the Δ*vprh*/Δ*hns1* or Δ*vprh*/Δ*hns1*/T6SS1^{-} strains (**Figure 4d,e**).

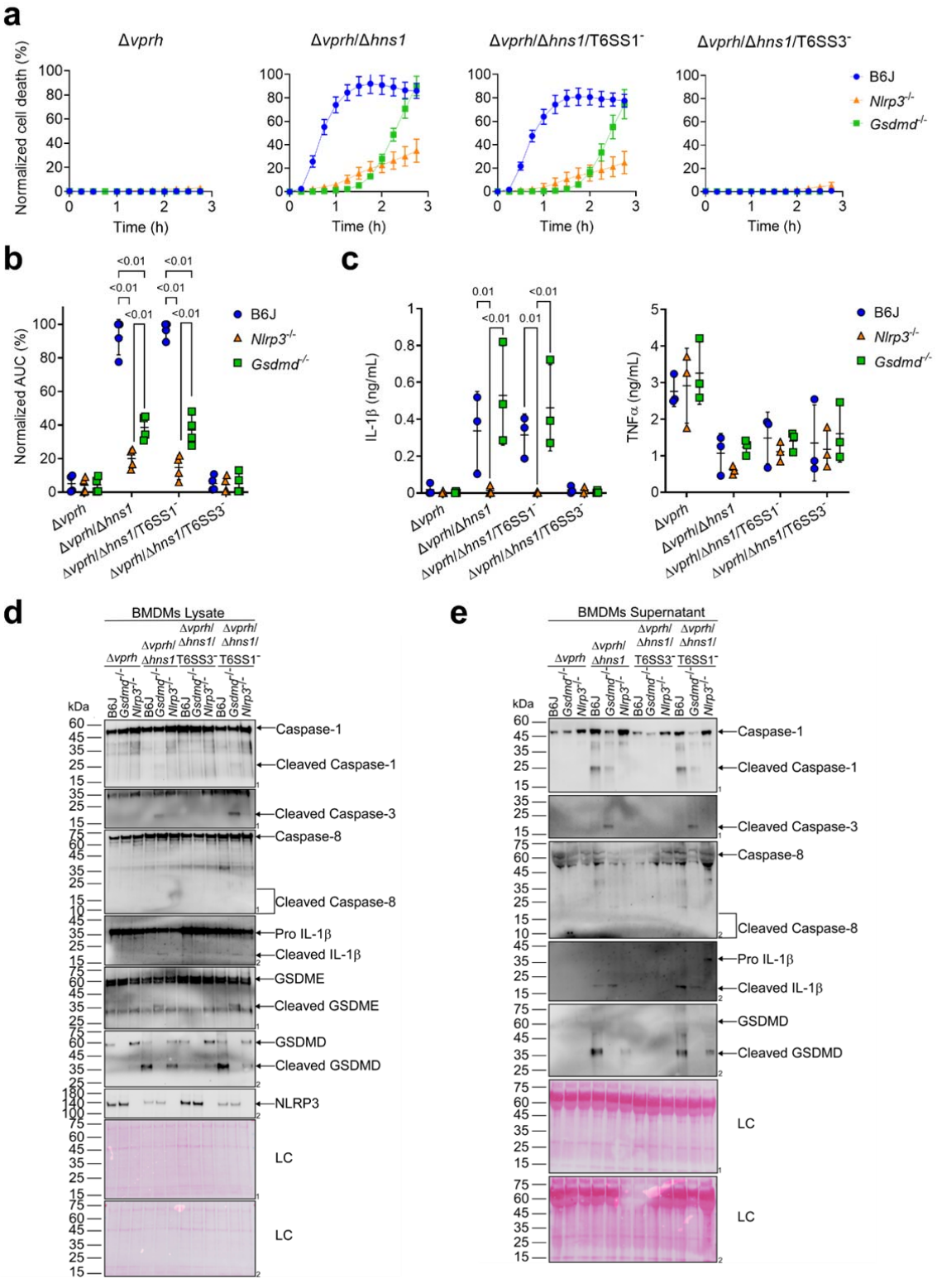

Figure 4: GSDME partially compensates for GSDMD absence in T6SS3-induced pyroptosis and IL-1β secretion

Approximately 3.5*10^4 wild-type (B6J), *Nlrp3*$^{-/-}$ and *Gsdmd*$^{-/-}$ BMDMs were seeded into 96-well plates in 6 replicates and were primed using LPS (100 ng/mL) for 3 hours prior to infection with *V. proteolyticus* strains at MOI 5. **(a-b)** PI uptake was assessed using real-time microscopy (IncucyteZOOM) (a) and then graphed as the AUC of the percentage of PI-positive cells normalized to the number of cells in the wells (b). **(c)** Cell supernatants described in (a) were collected 3 hours post infection. IL-1β and TNFα secretion were measured using commercial ELISA kits. **(d-e)** NLRP3, Caspase-1, Caspase-3, Caspase-8, GSDMD, GSDME, and IL-1β were detected in BMDM lysate (d) and supernatant (e) by immunoblotting (the number on the right side of each blot denotes the blot number). Arrows denote the expected band size;] denote the expected band sizes for cleaved Caspase-8. The data in (a) represent n≥3 independent experiments. Statistical comparisons in (b-c) between the different treatments were performed using RM two-way ANOVA, followed by Turkey's multiple comparison test. The results in (b,c) are shown as the mean ± SD of n≥3 independent experiments; significant differences (P<0.05) are denoted only for comparisons between mice strains infected with the same bacterial strain. The results shown in (d-e) represent 2 independent experiments.

Activation of T6SS3 by Ats3 is sufficient to induce the NLRP3 inflammasome

The above-mentioned T6SS3-dependent activation of the NLRP3 inflammasome was observed upon infection of BMDMs with bacterial strains harboring a deletion in *hns1*. Since H-NS is a global repressor (Dorman, 2004), and thus the deletion of *hns1* may have affected additional cellular systems other than T6SS1 and T6SS3, we set out to identify a positive regulator of T6SS3 that can be used to induce T6SS3, without affecting the activity of T6SS1.

VPR01S_RS02370 is found at the edge of the T6SS3 gene cluster (**Figure 5a**), and it is transcribed in the opposite direction from its neighboring T6SS3 cluster gene, *VPR01S_RS*02375. *VPR01S_RS02370* encodes a predicted transcription regulator belonging to the GlxA superfamily (according to the NCBI Conserved Domain Database (Lu et al., 2020)). The proximity of *VPR01S_RS02370* to the

T6SS3 cluster, and the absence of a recognizable transcription regulator within the cluster led us to hypothesize that this gene, henceforth referred to as *ats3* (**a**ctivator of **t**ype **s**ix secretion system **3**), regulates T6SS3. To test this hypothesis, we introduced *ats3* on an arabinose-inducible expression plasmid into the Δ*vprh* and Δ*vprh*/T6SS3^{-} strains, and determined its effect on T6SS1 and T6SS3 activity. Importantly, we found that T6SS3 was dramatically induced upon Ats3 over-expression, as evident by elevated expression and secretion of Hcp3, whereas T6SS1 activity (determined by monitoring VgrG1 expression and secretion) remained unaltered (**Figure 5b**). Remarkably, over-expression of Ats3 had a stronger effect on T6SS3 activity than deletion of *hns1* (**Figure 5b**). These results suggest that Ats3 activates T6SS3 and not T6SS1.

Previous work showed that T6SS1 alone was responsible for *V. proteolyticus*'s antibacterial activity during interbacterial competition (Ray et al., 2017). To further confirm that Ats3 affects T6SS3 and not T6SS1, we determined whether Ats3 over-expression results in enhanced T6SS1-mediated antibacterial activity. Interbacterial competition assays against sensitive *E. coli* prey (Ray et al., 2017) revealed that in contrast to the enhanced antibacterial activity seen upon deletion of *hns1*, which induces both T6SS1 and T6SS3, over-expression of Ats3 had no effect on the antibacterial activity (**Figure 5c**). Furthermore, over-expression of Ats3 did not confer antibacterial activity to a strain in which T6SS1 was inactivated (Δ*vprh*/T6SS1^{-}). Taken together, these results indicate that Ats3 is a positive regulator of T6SS3, and that T6SS3 does not play a role in interbacterial competition.

We reasoned that Ats3 can be used to uncouple the effect of T6SS3 on pyroptosis induction from T6SS1 activity. Therefore, to confirm the specific role of T6SS3 in pyroptosis induction, we set out to investigate the effect of Ats3 over-

389 expression on inflammasome activation and cell death. Using real-time microscopy,
390 we found that over-expression of Ats3 from a plasmid (pAts3) induced a rapid,
391 T6SS3-dependent cell death in BMDMs, which was similar to that induced upon
392 *hns1* deletion (**Figure 5d,e & Figure SF2a**). Moreover, infection of *Nlrp3*$^{-/-}$ BMDMs
393 with Δ*vprh* bacteria carrying pAts3 resulted in reduced cell death compared to that
394 observed upon infection of BMDMs generated from WT mice. In agreement, IL-1β,
395 Caspase-1, and GSDMD cleavage and release were also induced, in a T6SS3-
396 dependent manner, upon Ats3 over-expression (**Figure 5f,g & Figure SF2b**); in
397 contrast, TNFα secretion was not affected by either of *V. proteolyticus* strains in both
398 WT and *Nlrp3*$^{-/-}$ BMDMs (**Figure 5f**). Notably, Ats3 over-expressing bacteria induced
399 a slow, NLRP3-independent cell death deficient in IL-1β, Caspase-1, and GSDMD
400 cleavage; this result suggests that another cell death mechanism could have been
401 induced upon T6SS3 activation in the absence of NLRP3 (**Figure 5e-g & Figure**
402 **SF2b**). The apparent cell death in BMDMs is probably not a result of a fitness
403 difference between *V. proteolyticus* strains, since we did not detect any difference in
404 either bacterial growth or motility (**Figure SF2c,d**). Combined, these results confirm
405 that T6SS3 is specifically responsible for the inflammasome-mediated cell death
406 induction in BMDMs.

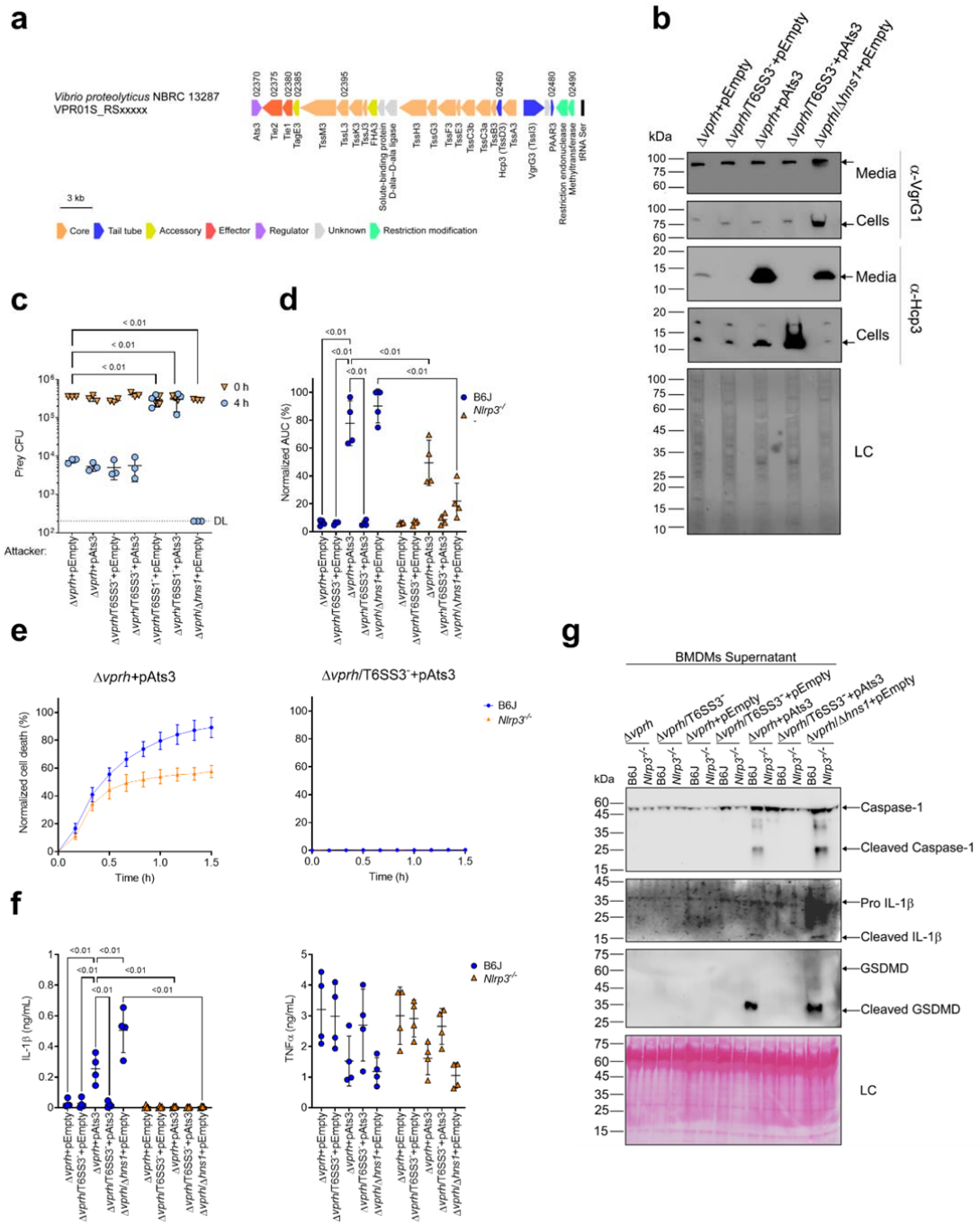

Figure 5: Activation of T6SS3 by Ats3 is sufficient to induce the NLRP3 inflammasome

(a) The T6SS3 gene cluster. Genes are represented by arrows indicating direction of transcription. Locus tags (*vpr01s_RSxxxxx*) are denoted above; encoded proteins and known domains are denoted below. **(b)** The expression (cells) and secretion (media) of Hcp3 and VgrG1 were detected by immunoblotting using specific

antibodies against Hcp3 and VgrG1, respectively. Loading control (LC) is shown for total protein lysate. **(c)** Viability counts of *E. coli* XL-1 Blue prey before (0 h) and after (4 h) co-incubation with the indicated attackers, on media containing 3% (w/v) NaCl and 0.1% (w/v) arabinose at 30°C. **(d-g)** Approximately $3.5*10^4$ wild-type (B6J) and *Nlrp3*$^{-/-}$ BMDMs were seeded into 96-well plates in 6 replicates and were primed using LPS (100 ng/mL) for 3 hours prior to infection with *V. proteolyticus* strains at MOI 5. Arabinose (0.05% w/v) was added to the media prior bacterial infection. (d-e) PI uptake was assessed using real-time microscopy (IncucyteZOOM) and then was graphed as the AUC of the percentage of PI-positive cells normalized to the number of cells in the wells. (f) Cell supernatants from experiments described in (a) were collected 3 hours post infection. IL-1β and TNFα secretion were measured using commercial ELISA kits. (g) NLRP3, Caspase-1, GSDMD, and IL-1β were detected in BMDM supernatants by immunoblotting. Arrows denote the expected band size. The data in (b-c, e) and (g) represent the results of n≥3 and n=2 independent experiment, respectively. The data in (c) are shown as the mean ± SD. Statistical comparisons in (c) between samples at the 4 h timepoint were performed using an unpaired, two-tailed Student's *t*-test; significant differences (P<0.05) are denoted above. DL, assay detection limit. Statistical comparisons in (d) and (f) between the different treatments were performed using RM two-way ANOVA, followed by Turkey's multiple comparison test. The results are shown as the mean ± SD of n≥4 independent experiments; significant differences (P<0.05) are denoted for comparisons between infections of cells from the same mouse strain, and between infections using the same *V. proteolyticus* strain.

T6SS3-induced pyroptosis requires bacterial internalization

Previous reports suggested that for some T6SSs, delivery of anti-eukaryotic effectors requires internalization by a host cell (Ma et al., 2009; Shalom et al., 2007). This phenomenon was also observed for the *V. proteolyticus* T6SS1-mediated manipulation of the actin cytoskeleton (Ray et al., 2017). Therefore, we asked whether the T6SS3-mediated phenotypes observed upon infection of BMDMs are dependent on phagocytosis. Indeed, we found that the addition of cytochalasin D,

445 which inhibits phagocytosis by inhibiting actin polymerization (Brown and Spudich,
446 1979; Flanagan and Lin, 1980), abolished the pyroptosis induced by the T6SS3 of a
447 Δ*vprh V. proteolyticus* strain over-expressing Ats3 (**Figure 6a & Figure SF3a**).
448 Interestingly, cytochalasin D also abolished the weaker inflammasome-independent,
449 T6SS3-dependent cell death observed upon infection of *Nlrp3*$^{-/-}$ BMDMs. Notably,
450 cytochalasin D did not abolish the cell death induced by T3SS1 of another pathogen,
451 *V. parahaemolyticus*, which is independent of bacterial internalization (Burdette et
452 al., 2008) and was therefore used as a control (**Figure SF3b**); it also did not impair
453 bacterial growth (**Figure SF3c**). Combined, these results suggest that the T6SS3-
454 mediated pyroptotic cell death requires phagocytosis.

455 Phagocytic cells, such as BMDMs, internalize bacteria to eliminate them. We
456 reasoned that *V. proteolyticus* activate the T6SS3 upon phagocytosis because this
457 system provides a survival advantage. Indeed, when we measured the bacterial load
458 after 3 hours of BMDM infection, we observed a dramatic advantage for *V.*
459 *proteolyticus* with an active T6SS3 (Δ*vprh*+pAts3; parental strain) over a derivative
460 strain with an inactive T6SS3 (T6SS3^{-}) (**Figure 6b**). Notably, bacterial counts were
461 comparable between the two strains in the absence of BMDMs (**Figure 6b**).
462 Remarkably, the presence of BMDMs appeared to provide a growth advantage to
463 bacteria with an active T6SS3 or to bacteria that were not phagocytosed by BMDMs
464 (i.e., in the presence of cytochalasin D), whereas bacteria with an inactive T6SS3
465 that were phagocytosed (i.e., in the absence of cytochalasin D) grew less than their
466 counterparts in the absence of BMDMs (**Figure 6b**). Taken together, these results
467 demonstrate that T6SS3 provides a survival advantage to *V. proteolyticus* upon its
468 internalization by an immune cell.
469

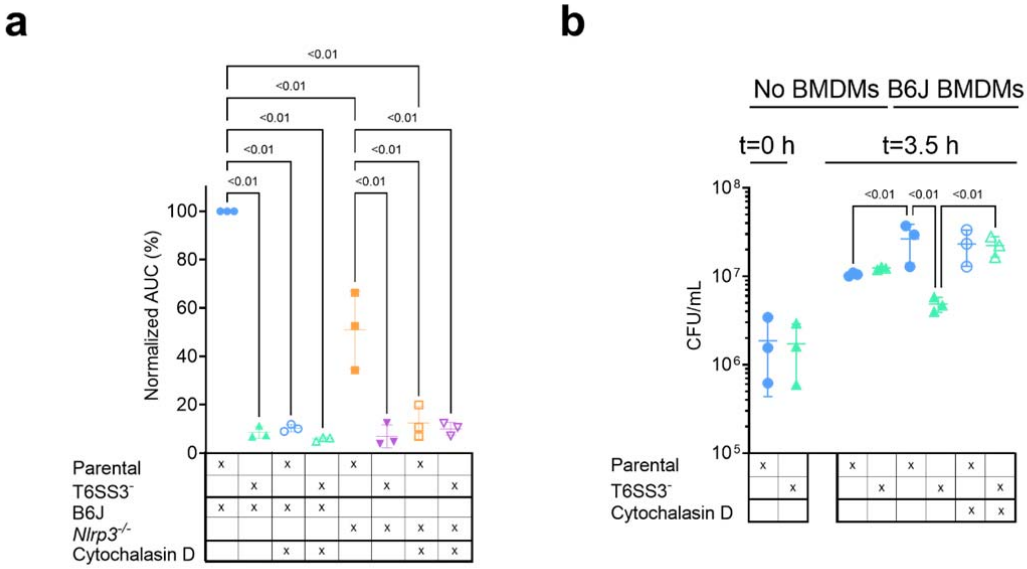

Figure 6: *V. proteolyticus* T6SS3-induced pyroptosis requires phagocytosis

Approximately 3.5*10^4 wild-type (B6J) and *Nlrp3*$^{-/-}$ BMDMs were seeded into 96-well plates in n ≥ 3 replicates and were primed using LPS (100 ng/mL) for 3 hours prior to infection with *V. proteolyticus* strains at MOI 5. Arabinose (0.05% w/v) was added to the media prior to bacterial addition. When indicated, cytochalasin D (5 µM) was added to the cells 45 minutes prior to bacterial infection. **(a)** PI uptake was assessed using real-time microscopy (IncucyteZOOM) and then graphed as the AUC of the percentage of PI-positive cells normalized to the number of cells in the wells. **(b)** bacterial counts of *V. proteolyticus* strains before (t=0 h) and after (t=3.5 h) BMDMs infection C. The results in (a,b) are shown as the mean ± SD of n=3 independent experiments. Statistical comparisons in (a) between the different treatments were performed using RM one-way ANOVA, followed by Sidak multiple comparison test. Statistical comparison in (b) between the different treatments were performed using RM one-way ANOVA. Significant differences (P<0.05) are denoted. Parental, *V. proteolyticus* Δ*vprh*+pAts3; T6SS3$^-$, *V. proteolyticus* Δ*vprh*/Δ*tssL3*+pAts3.

Two T6SS3 effectors are necessary and sufficient to induce pyroptotic cell death

While analyzing the T6SS3 gene cluster, we were intrigued by two genes found adjacent to *ats3*, namely, *VPR01S_RS02380* and *VPR01S_RS02375* (**Figure 5a**). The two genes, hereafter termed *tie1* (T6SS3 inflammasome-inducing effector 1) and *tie2*, respectively, encode proteins with no apparent similarity to known T6SS core or accessory components (Boyer et al., 2009). Interestingly, hidden Markov model analyses (using the Jackhmmer server (Potter et al., 2018)) revealed that Tie2 shares partial similarity (in the region between amino acids 326 and 469) with domains found at C-termini of polymorphic toxins, such as proteins containing N-terminal LXG and WXG100 domains that are associated with type VII secretion systems (Tran et al., 2021; Whitney et al., 2017), as well as DUF4157 domains, which were recently suggested to carry toxins in extracellular contractile injection systems (Geller et al., 2021). These observations led us to hypothesize that Tie1 and Tie2 are T6SS3 effectors. To test this hypothesis, we generated custom-made antibodies against Tie1 and Tie2, and monitored their expression and secretion upon over-expression of Ats3, which activates T6SS3. As shown in **Figure 7a**, Tie1 and Tie2 were secreted in a T6SS3-dependent manner, as was Hcp3; in contrast, secretion of VgrG1, a T6SS1 component, was unaffected by Ats3 over-expression. These results confirm that both Tie1 and Tie2 are T6SS3 secreted proteins.

The above findings prompted us to posit that if Tie1 and Tie2 are indeed T6SS3 effectors, then they can be responsible for the T6SS3-mediated induction of pyroptosis in BMDMs. To test this hypothesis, we generated *V. proteolyticus* mutant strains with deletions in either *tie1* (deletion of the region corresponding to nucleotides 485-584 in *tie1*), *tie2*, or both; we used them to infect BMDMs, and then we monitored the effect on cell death. Remarkably, deletion of both *tie1* and *tie2* in a Δ*vprh*/Δ*hns1* background (Δ*vprh*/Δ*hns1*/Δ*tie1*/Δ*tie2*) completely abolished the cell

515 death and IL-1β secretion observed upon infection of BMDMs with the Δ*vprh*/Δ*hns1*
516 strain (**Figure SF3a,b**), without affecting TNFα secretion (**Figure SF3b**). Deletion of
517 *tie1* alone resulted in an intermediate cell death phenotype, whereas deletion of *tie2*
518 alone had no significant effect. Complementation of Tie1 and Tie2 expression from a
519 plasmid in the Δ*vprh*/Δ*hns1*/Δ*tie1*/Δ*tie2* strain revealed that over-expression of Tie1,
520 either alone (pTie1) or together with Tie2 (pTie1-2), completely restored the cell
521 death phenotype, whereas bacteria over-expressing only Tie2 (pTie2) regained an
522 intermediate ability to induce cell death (**Figure 7b,c**). Similar effects of *tie1* and *tie2*
523 deletions were observed in the tested inflammasome-activation hallmark
524 phenotypes, including IL-1β, Caspase-1, and GSDMD cleavage and release (**Figure**
525 **7d-f & Figure SF3b-d**). TNFα secretion was not significantly affected by
526 complementation of Tie1 or Tie2 when BMDMs were infected with the indicated *V.*
527 *proteolyticus* strains (**Figure 7d**). Importantly, deletion of *tie1*, *tie2*, or both did not
528 affect T6SS3 functionality, as evident by the secretion of Hcp3 (**Figure SF3e**); it also
529 did not affect bacterial growth or swimming motility (**Figure SF3f-g**). Taken together,
530 these results indicate that Tie1 and Tie2 are T6SS3 effectors that are necessary to
531 induce inflammasome-mediated cell death in BMDMs. Either protein is also sufficient
532 to induce cell death, although the effect of Tie1 is more pronounced than that of
533 Tie2.

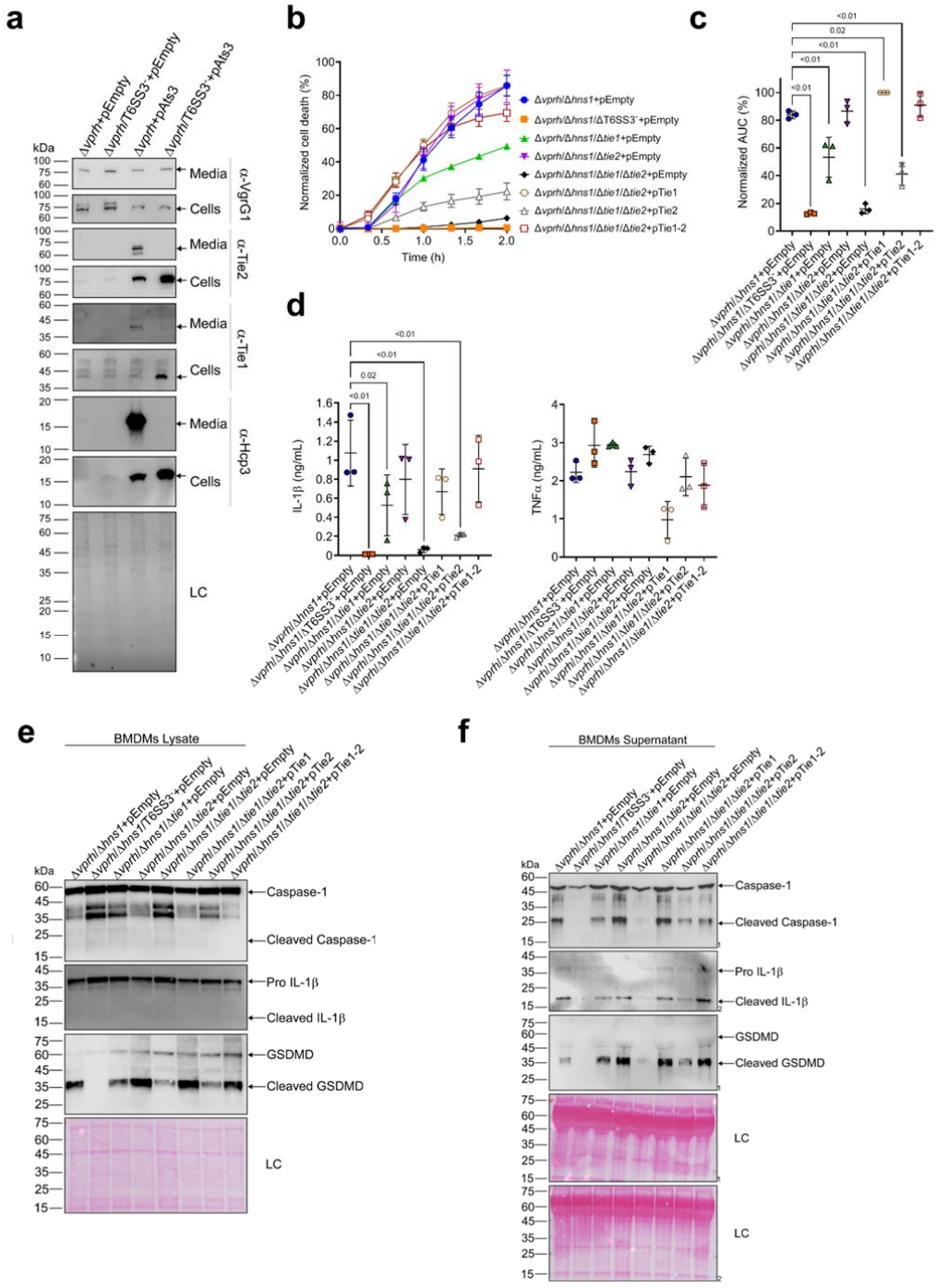

Figure 7: Two T6SS3 effectors are necessary and sufficient to induce pyroptosis

(a) The expression (cells) and secretion (media) of Tie1, Tie2, Hcp3 and VgrG1 from *V. proteolyticus* strains were detected by immunoblotting using custom-made antibodies. Loading control (LC) is shown for total protein lysate. **(b-f)** Approximately

3.5*10^4 wild-type BMDMs were seeded into 96-well plates in 6 replicates and were primed using LPS (100 ng/mL) for 3 hours prior to infection with *V. proteolyticus* strains at MOI 5. Arabinose (0.05% w/v) and 250 µg/mL kanamycin were added to the media prior to bacterial infection. **(b-c)** PI uptake was assessed using real-time microscopy (IncucyteZOOM) (b) and then graphed as the AUC of the percentage of PI-positive cells normalized to the number of cells in the wells (c). **(d)** Cell supernatants from experiments described in (b) were collected 3 hours post infection. IL-1β and TNFα secretion were measured using commercial ELISA kits. **(e-f)** NLRP3, Caspase-1, GSDMD, and IL-1β were detected in BMDM lysates (e) and supernatants (f) by immunoblotting. The data in (a-b) and (e-f) represent 3 and 2 independent experiments, respectively. Statistical comparisons in (c-d) between the different treatments were performed using RM one-way ANOVA, followed by Dunnett's multiple comparison test. The results are shown as the mean ± SD of 3 independent experiments; significant differences (P<0.05) are denoted only for comparisons of treatments to the Δ*vprh*/Δ*hns1*+pEmpty treatment. In (a, e, f), arrows denote the expected band size.

T6SS3-like systems are found in pathogenic marine bacteria

Since vibrios are known for their ability to share traits and virulence factors via horizontal gene transfer (HGT) (Roux et al., 2015), we asked whether T6SS3-like clusters are found in other bacteria. Indeed, we identified highly similar T6SS clusters in other marine bacteria, including human pathogens such as *V. parahaemolyticus* and *V. vulnificus* (Baker-Austin et al., 2018), and marine animal pathogens such as *Vibrio crassostreae* (Bruto et al., 2017) and *Vibrio anguillarum* (Frans et al., 2011) (**Figure 8**). Interestingly, these T6SS3-like clusters are often adjacent to mobile genetic elements such as integrases or transposases, suggesting a mechanism for their spread via HGT. Notably, the identified T6SS3-like clusters carry a homolog of at least one of the inflammasome-inducing effectors, Tie1 or

Tie2, at the edge of the cluster. Thus, these systems probably maintain their inflammasome-inducing activity, which may contribute to their pathogenic potential.

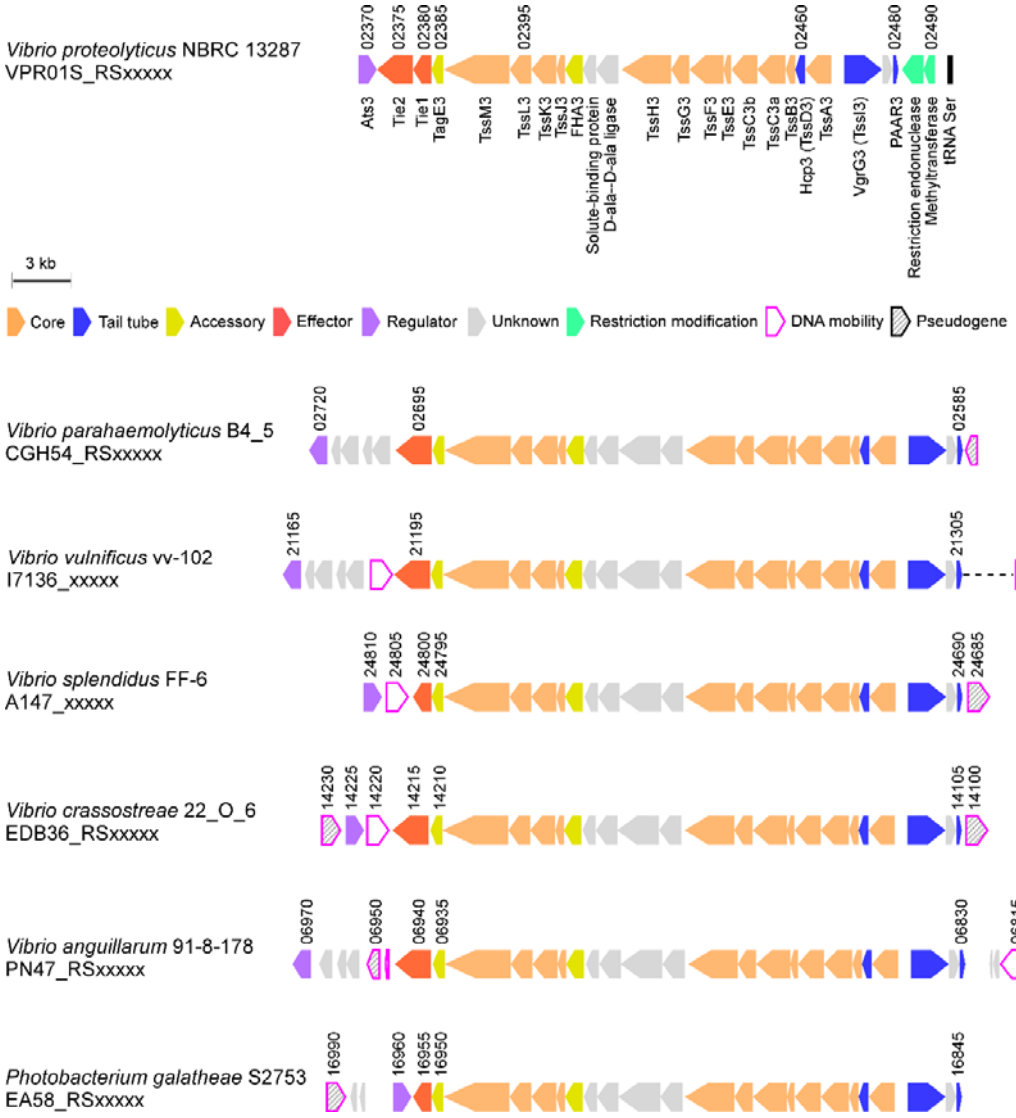

Figure 8: T6SS3-like systems are found in pathogenic marine bacteria

T6SS3-like gene clusters. Genes are represented by arrows indicating the direction of transcription. Locus tags are denoted above; encoded proteins and known domains are denoted below for *V. proteolyticus*. A dashed line denotes a gap containing genes that are not shown.

Discussion

T6SSs are sophisticated molecular machines that are used by Gram-negative bacteria to inject toxic effector proteins into neighboring cells. Even though most T6SSs studied to date mediate interbacterial competition by injecting antibacterial effectors into neighboring bacteria, few T6SSs were found to target eukaryotes (Bröms et al., 2010; Clemens et al., 2018; Jiang et al., 2014; Monjarás Feria and Valvano, 2020; Pukatzki et al., 2007; Rosales-Reyes et al., 2012; Sana et al., 2015; Wang et al., 2009). In this work, we describe T6SS3, a functional T6SS in the marine bacterium *V. proteolyticus*, which induces inflammasome-mediated cell death (known as pyroptosis) upon phagocytosis. We show that this T6SS-mediated pyroptotic cell death is dependent on the delivery at least two novel effectors, and that it involves the activation of the NLRP3 inflammasome, leading to the processing and release of Caspase-1, IL-1β, and GSDMD. Two other T6SS effectors were previously reported to indirectly affect inflammasome activation: EvpP from *Edwardsiella tarda* was shown to inhibit the NLRP3 inflammasome by targeting the MAPK-Jnk pathway (Chen et al., 2017), whereas TecA from *Burkholderia cenocepacia* deamidates Rho GTPases, leading to activation of the pyrin-inflammasome (Aubert et al., 2016). Here, we describe for the first time, to the best of our knowledge, not one but two T6SS effectors that lead to activation of the NLRP3 inflammasome.

Remarkably, we found that in the absence of GSDMD, the canonical gasdermin activated during pyroptosis, an alternative NLRP3-dependent inflammasome cell death cascade, which includes Caspase-3 (but not Caspase-8) and GSDME, can be induced by this T6SS3. Since IL-1β release is one of the most ancient and conserved immune mechanism (Dinarello, 2018), it is impotent to understand how

604 the mammalian immune system evolved to induce several backup mechanisms to
605 ensure its activation. Even in the case of GSDMD inhibition, which may occur if
606 GSDMD is targeted by the pathogen (Luchetti et al., 2021), a conserved mechanism
607 including the activation of Caspase-3 and GSDME in a NLRP3 inflammasome-
608 dependent manner will result in the secretion of this proinflammatory cytokine.
609 Notably, a recent study independently reported a similar compensation mechanism
610 in the absence of GSDMD via chemical or *Salmonella*-induced NLRP3
611 inflammasome activation that also included Caspase-8 activation (Zhou and Abbott,
612 2021). In contrast, we were unable to detect Caspase-8 activation in our system.
613 Notably, a recent study independently reported a similar compensation mechanism
614 in the absence of GSDMD via chemical or *Salmonella*-induced NLRP3
615 inflammasome activation; the reported mechanisms also included Caspase-8
616 activation (Zhou and Abbott, 2021). In contrast, we were unable to detect Caspase-8
617 activation in our system. Therefore, we propose that the cascade revealed in our
618 work involves direct Caspase-3 activation by Caspase-1, as was previously
619 suggested for Aim2 inflammasome in the absence of Caspase-8 (Sagulenko et al.,
620 2018).

621 In the battle between mammalian cells and pathogens, the immune response
622 mechanism that is activated plays a central role in the host's ability to fight-off
623 infections. Inflammasome activation (and pyroptotic cell death), which is an ancient
624 innate immune mechanism, is activated by numerous inputs and cellular stresses
625 (Lamkanfi and Dixit, 2014; Schroder and Tschopp, 2010). Nevertheless, the
626 immunological consequences of inflammasome activation by pathogens remain
627 enigmatic. Often it is a useful mechanism that enables the host to eliminate infection
628 either by inducing inflammation or by killing infected cells; however, in certain

scenarios, inflammasome activation can be exploited by the pathogen, and it provides it with an advantage against the immune system (Man et al., 2017). Indeed, we observed a T6SS3-mediated growth advantage to *V. proteolyticus* during BMDMs infection when phagocytosis, which is generally used by the immune cell to eliminate the bacteria, was functional. Future investigations will determine whether T6SS3-induced pyroptosis is beneficial to the bacterium or to the host during in vivo infection.

Although mammals are probably not the natural target for the *V. proteolyticus* T6SS3, nor are they the evolutionary driving force for the activity of the effectors Tie1 and Tie2, immune responses similar to the ones described here (e.g., cell death mechanisms) are found in marine animals that are in direct contact with pathogenic vibrios (e.g., arthropods and fish). Indeed, *Vibrio coralliilyticus* was recently described to activate Caspase-3, leading to cleavage of GSDME and cell death in corals (Jiang et al., 2020), while a Caspase-1 homolog was previously described in *Artemia sinica* (Chu et al., 2014). Since NLR proteins, such as NLRP3, are less conserved in marine animals, we hypothesize that the target of Tie1 and Tie2 is upstream of NLRP3, and therefore the conservation between mammalian cells and marine animals lies in their ability to sense the effect of Tie1 and Tie2 activity as a danger signal that activates cell death pathways. Moreover, since we find homologous T6SS clusters that carry Tie1 and Tie2 homologs in other bacteria, including human pathogens, this T6SS and these effectors may contribute to the virulence of some bacteria. Finally, the probable horizontal transfer of this anti-eukaryotic T6SS between marine bacteria may also contribute to the emergence of new pathogenic *Vibrio* strains.

Here, we also shed light on the regulation of T6SS3. We found that similar to T6SS in other bacteria, both T6SS1 and T6SS3 in *V. proteolyticus* are repressed by H-NS. Importantly, we demonstrated that Ats3, which appears to be conserved also in the homologous T6SS clusters found in other bacteria, is an activator of T6SS3 but not of T6SS1. When over-expressed, Ats3 activated T6SS3 even more dramatically than the deletion of *hns1*. Interestingly, the Ats3-induced T6SS3 activated NLRP3 independent cell death in BMDMs, which had different kinetics than the NLRP3-mediated cell death. This result suggests that upon hyper-activation, T6SS3 can induce different cell death mechanisms.

In conclusion, we describe T6SS3, an anti-eukaryotic T6SS in *V. proteolyticus*, and we identify two novel anti-eukaryotic effectors. We also decipher the mechanism of cell death, which is induced by the two effectors in primary macrophages. Nevertheless, future studies will address the question regarding the activity and target of the two effectors, and they will determine how these effectors activate the inflammasome. Moreover, it remains to be determined whether inflammasome-induced cell death is beneficial to the host or to the bacterium during infection.

Acknowledgements

This work was performed in partial fulfillment of the requirements for a Ph.D. degree for (H.C), the Sackler Faculty of Medicine, Tel Aviv University, Israel. C.M.F was supported by a scholarship from the Clore Israel Foundation, a scholarship for outstanding doctoral students from the Orthodox community (The Council for Higher Education), and by a fellowship from the Manna Center Program in Food Safety and Security at Tel Aviv University. The research of D.S. and M.G. was supported by the

677 Israel Science Foundation (ISF) (grants 920/17 and 2174/22), and the Recanati
678 Foundation (TAU).

679

680 **Author contributions**

681 Conceptualization, D.S., and M.G.; Methodology, H.C., N.B., C.M-F., L.E-B., D.S.,
682 and M.G.; Investigation, H.C., N.B., L.E-B., D.S., and M.G.; Writing – Original Draft,
683 H.C,; Writing – Review & Editing, H.C., D.S., and M.G.; Funding Acquisition, D.S.,
684 and M.G.; Validation, H.C., N.B.; Supervision, D.S., and M.G.

685

686 **Declaration of interests**

687 The authors declare no competing interests.

Material and Methods

Reagents

Unless otherwise stated, all cell culture reagents were purchased from Biological Industries, Beit-Haemek, Israel. Lipopolysaccharides (LPS) of *Escherichia coli* O111:B4 were purchased from Sigma-Aldrich (#L3024). Propidium Iodide (PI) was purchased from Sigma-Aldrich (#P4170). Vx765 and MCC950 and ELISA kits were purchased from Invitrogen. HRP-conjugated secondary antibodies were purchased from Jackson ImmunoResearch Labs (West Grove, PA, USA). Cytochalsin D (1233) was purchased from Tocris.

Mice: C57BL/6 (wild-type [WT]), NLRP3tm1Bhk/J, MLKL KO, NLRP1 KO and GSDMD KO mice were bred under specific pathogens free conditions in the animal facility at Tel Aviv University. Experiments were performed according to the guidelines of the Institute's Animal Ethics Committees.

Cell culture: Bone marrow (BM) cells from mice were isolated by flushing femurs and tibias with 5 mL PBS supplemented with 2% (v/v) heat-inactivated fetal bovine serum (FBS) Gibco (Thermo Fisher Scientific, Waltham, MA, USA). The BM cells were centrifuged for 5 minutes at 400 x *g* and then resuspended in Dulbecco's Modified Eagle Medium (DMEM) (Sartorius, 01-052-1A) supplemented with 10% (v/v) FBS and 15% L929 conditional medium (L-con). Bone marrow-derived macrophages (BMDMs) were obtained by 7 days differentiation as previously described (Trouplin et al., 2013).

Bacterial strains and media: For a complete list of strains used in this study, see **Supplemental Table S1**. *Vibrio proteolyticus* and its derivatives, as well as *V. parahaemolyticus*, were grown in Marine Lysogeny Broth (MLB; Lysogeny broth

supplemented with NaCl to a final concentration of 3% [w/v]) or on MLB agar plates (supplemented with 1.5% [w/v] agar) at 30°C. Media were supplemented with kanamycin (250 µg/mL) or chloramphenicol (10 µg/mL) when appropriate to maintain plasmids. *Escherichia coli* were grown in 2xYT broth (1.6% [w/v] tryptone, 1% [w/v] yeast extract, and 0.5% [w/v] NaCl) or Lysogeny broth (LB) at 37°C. Media were supplemented with kanamycin (30 µg/mL) or chloramphenicol (10 µg/mL) when appropriate to maintain plasmids. To induce the expression of genes from pBAD plasmids, 0.1% (w/v) L-arabinose was included in the media.

Plasmid construction: For a complete list of plasmids used in this study, see **Supplemental Table S2**. Primers used for amplification are listed in **Supplemental Table S3**. For arabinose-inducible expression, the coding sequences (CDS) of *tssL3*, *ats3*, *tie1* and *tie2* were amplified from *V. proteolyticus* genomic DNA. Amplicons were inserted into the multiple cloning site (MCS) of pBAD/Myc-His^{Kan} using the Gibson-assembly method (Gibson et al., 2009). The constructed plasmids were transformed into *E. coli* DH5α (λ-pir) competent cells using electroporation. Plasmids were conjugated into *V. proteolyticus* using tri-parental mating. Trans-conjugants were selected on MLB agar plates supplemented with appropriate antibiotics to maintain the plasmids.

Construction of bacterial deletion strains: For in-frame deletions of *V. proteolyticus* genes, 1 kb sequences upstream and downstream of each gene or region to be deleted were cloned into pDM4, a CmROriR6K suicide plasmid (O'Toole et al., 1996) using restriction digestion and ligation. These pDM4 constructs were transformed into *E. coli* DH5α (λ-pir) by electroporation, and then transferred into *V. proteolyticus* via conjugation. Trans-conjugants were selected on MLB agar plates containing chloramphenicol (10 µg/mL). The resulting trans-conjugants were grown

738 on MLB agar plates containing sucrose (15% [w/v]) for counter-selection and loss of
739 the SacB-containing pDM4. Deletion was confirmed by PCR.

740 **Bacterial growth assays:** Overnight-grown cultures of *V. proteolyticus* were
741 normalized to an OD_{600} = 0.01 in MLB media and transferred to 96-well plates (200
742 µL per well). For each experiment, n = 3. Cultures were grown at 30°C or 37°C in a
743 BioTek EPOCH2 microplate reader with continuous shaking at 205 cpm. OD_{600}
744 readings were acquired every 10 minutes. Experiments were performed at least
745 three times with similar results.

746 **Bacterial swimming assays:** Swimming media plates were prepared with Lysogeny
747 broth containing 20 g/L NaCl and 3 g/L Agar. When necessary to induce the
748 expression of genes from a plasmid, 0.1% (w/v) L-arabinose was included in the
749 media. *V. proteolyticus* strains that were grown overnight on an MLB plate were
750 picked and then stabbed into the swimming plates using a toothpick (n = 3). Plates
751 were incubated at 30°C for 8–16 h. Swimming was assessed by measuring the
752 diameter of the spreading bacterial colony. The experiments were performed three
753 times with similar results.

754 **Infection experiments:** BMDMs were washed three times using PBS and then
755 seeded at a final concentration of $3.5*10^4$ cells/mL in triplicate in 1% FBS and
756 penicillin–streptomycin-free DMEM. BMDMs were pre-incubated with LPS (100
757 ng/mL, 3 h), and then infected with *V. proteolyticus* at MOI 5. When used,
758 inflammasome inhibitors Vx765 (25 µM) and MCC950 (2 µM) were added 30
759 minutes prior to infection. For phagocytosis inhibition assay, cytochalasin D (final
760 concentration 5 µM) was added 30 minutes prior to infection. More specifically,
761 overnight cultures of *V. proteolyticus* strains were washed and normalized to
762 OD_{600}=0.016 (5 MOI) in DMEM without antibiotics. Bacteria were added to wells

763 containing the BMDMs, and plates were centrifuged for 5 minutes at 400 x *g*. Plates
764 were inserted into the IncucyteZOOM (Essen BioScience) for incubation at 37°C and
765 for monitoring cell death, as detailed below.
766 **Live cell imaging**: Plates containing BMDMs were placed in IncucyteZOOM and
767 images were recorded every 10–30 minutes. The data were analyzed using the
768 IncucyteZoom2016B analysis software and then exported to the GraphPad Prism
769 software. Normalization was performed according to the maximal PI-positive object
770 count to calculate the percentage of dead cells (Isherwood et al., 2011).
771 **Immune response immunoblot analyses:** Cells were collected and pelleted by
772 centrifugation for five minutes at 400 x *g* (4°C). Next, the cells were lysed by adding
773 denaturing (2X) Tris-Glycine SDS Sample Buffer supplemented with 5% (v/v) β-
774 mercaptoethanol. Lysates were loaded onto any-kD gradient ExpressPlus™ Page
775 precast gels (GenScript). Proteins were transferred onto a nitrocellulose membrane
776 (Bio-Rad), and Ponceau S staining was performed routinely to evaluate the loading
777 accuracy. Membranes were blocked with 5% (w/v) skim milk in Tris-Buffered
778 Saline(TBS) for 1-2 h, and then probed overnight with primary antibodies (all
779 antibodies were diluted 1:1000, unless noted otherwise): mouse-NLRP3 (AdipoGen;
780 cryo-2), pro and mature mouse-IL-1β (R&D Systems; AF-401-NA), pro and cleaved
781 mouse Caspase-1 (Santa Cruz; sc- 514) (Adipogen; AG-20B-0042-C100), pro and
782 cleaved mouse-GSDMD (Abcam; ab209845), pro and cleaved mouse-GSDME
783 (Abcam, ab215191), cleaved Caspase-3 (Cell Signaling, 9661S) and Caspase-8
784 (R&D; AF1650). Relevant horseradish peroxidase-conjugated secondary antibodies
785 were applied for at least 1 h. Membranes were washed four times in TBS containing
786 0.1% (v/v) Tween 20 (TBST) between antibody incubations. Antibodies were diluted
787 in TBST containing 5% (w/v) skim milk. Immunoblots were visualized using an ECL

kit (Bio-Rad) in an ODYSSEY Fc (Li-COR) equipped with Image Lab software. All images were cropped for presentation; full-size images will be presented upon request.

Protein secretion assays: *V. proteolyticus* isolates were grown overnight in MLB broth supplemented with antibiotics to maintain plasmids, if needed. Cultures were normalized to $OD_{600} = 0.18$ in 5 mL MLB with appropriate antibiotics and 0.05% (w/v) arabinose, when required. Cultures were grown for 5 h at 30 °C. After 5 h, for expression fractions (cells), 0.5 OD_{600} units were collected, and cell pellets were resuspended in (2X) Tris-Glycine SDS sample buffer (Novex, Life Sciences). For secretion fractions (media), culture volumes equivalent to 10 OD_{600} units were filtered (0.22 µm), and proteins were precipitated using deoxycholate and trichloroacetic acid (Bensadoun and Weinstein, 1976). Cold acetone was used to wash the protein precipitates twice. Then, protein precipitates were resuspended in 20 µL of 10 mM Tris-HCl pH = 8, followed by the addition of 20 µL of (2X) Tris-Glycine SDS Sample Buffer supplemented with 5% (v/v) β-mercaptoethanol. Next, 0.5 µL of 1 N NaOH was added to maintain a basic pH. Expression and secretion samples were boiled and then resolved on any-kD gradient Mini-PROTEAN or Criterion™TGX Stain-Free™ precast gels (Bio-Rad). Expression and secretion were evaluated using western blot with specific, custom-made antibodies against VgrG1 (described previously(Li et al., 2017)), and Hcp3, Tie1, or Tie2 (polyclonal antibodies raised in rabbits against peptides: CQKHNYELEGGEIKD, CVNIGKKYTDFTEDEL, and STPLGKAVDIPVEKC, respectively). Tie2, Hcp3 and VgrG1 antibodies were used at 1:1000 dilution, and Tie1 antibodies were used at 1:5000 dilution. Protein signals were visualized in a Fusion FX6 imaging system (Vilber Lourmat) using

enhanced chemiluminescence (ECL) reagents. Equal loading was assessed using trihalo compounds' fluorescence of the immunoblot membrane.

Bacterial competition assays: Attacker and prey strains were grown overnight in appropriate broth (MLB for *V. proteolyticus* and 2xYT for *E. coli*) with the addition of antibiotics when maintenance of plasmids was required. Competition assays were performed as previously described (Salomon et al., 2013). Briefly, bacterial cultures were normalized to $OD_{600} = 0.5$ and were mixed at a 4:1 ratio (attacker:prey). Triplicates of mixtures were spotted (25 µL) on MLB agar plates containing 0.1% (w/v) arabinose, and incubated for 4 h at 30°C. Prey colony forming units (CFU) were calculated after the cultures from t=0 h and t=4 h were collected and grown on selective media plates. The assay was performed three times with similar results, and the results from representative experiments are shown.

Bacterial count quantification: BMDM infection experiments were performed as described above. Bacterial counts were assessed at the time of infection (t=0 h) and 3.5 h post infection (t=3.5 h). To recover bacteria, triton X-100 was added directly into the experiment wells to a final concentration of 1%, and the plate was incubated for 15 minutes at 37°C. The media were collected from the wells, and 10-fold serial dilutions were spotted onto selective media plates. CFU counts were determined after overnight incubation of the plates at 30°C. The assay was preformed three times with similar results.

Identification of T6SS3-homologous clusters: T6SS3-like clusters were identified by searching for homologs of the *V. proteolyticus* TssM3 protein sequence using BLAST (Stephen F.Altschul, Warren Gish, Webb Miller, Eugene W.Myers, 1990). The genomic neighborhoods of randomly selected homologs were then manually

836 examined, and representative clusters with similar genetic composition were chosen
837 for presentation.

838 **Statistical analysis:** Date were analyzed using GraphPad prism 9. Data are
839 presented as the mean ± standard deviation (SD). Comparisons was performed
840 using RM one-way ANOVA, followed by Sidak's multiple comparison test or RM two-
841 way ANOVA, followed by Tukey's multiple comparison test, unless otherwise is
842 indicated. Statistical significance was considered at $P < 0.05$.

843

844 **Supplemental Table S1. A list of bacterial strains used in this study.**

Strain name	**Genotype**	**Source**
Vibrio proteolyticus ATCC 15338	Wild-type	ATCC
T6SS1$^-$	*Vibrio proteolyticus* ATCC 15338 Δ*tssG1*	(Ray et al., 2017)
T6SS3$^-$	*Vibrio proteolyticus* ATCC 15338 Δ*tssL3*	This study
Δ*vprh*	*Vibrio proteolyticus* ATCC 15338 Δ*vprh*	(Ray et al., 2016)
Δ*vprh*/T6SS1$^-$	*Vibrio proteolyticus* ATCC 15338 Δ*vprh*/Δ*tssG1*	This study
Δ*vprh*/T6SS3$^-$	*Vibrio proteolyticus* ATCC 15338 Δ*vprh*/Δ*tssL3*	This study
Δ*vprh*/Δ*hns1*	*Vibrio proteolyticus* ATCC 15338 Δ*vprh*/ Δ*hns1*	This study
Δ*vprh*/Δ*hns1*/T6SS1$^-$	*Vibrio proteolyticus* ATCC 15338 Δ*vprh*/Δ*hns1*/Δ*tssG1*	This study
Δ*vprh*/Δ*hns1*/T6SS3$^-$	*Vibrio proteolyticus* ATCC 15338 Δ*vprh*/Δ*hns1*/Δ*tssL3*	This study
Δ*vprh*/Δ*hns1*/Δ*tie1*	*Vibrio proteolyticus* ATCC 15338 Δ*vprh*/Δ*hns1*/Δ*tie1*	This study

Δ*vprh*/Δ*hns1*/Δ*tie2*	*Vibrio proteolyticus* ATCC 15338 Δ*vprh*/Δ*hns1*/Δ*tie2*	This study
Δ*vprh*/Δ*hns1*/Δ*tie1*/Δ*tie2*	*Vibrio proteolyticus* ATCC 15338 Δ*vprh*/Δ*hns1*/Δ*tie1*/Δ*tie2*	This study
V. para	*V. parahaemolyticus* RIMD 2210633 *ΔtdhAS* derivative (strain POR1)	(Park et al., 2004)
Escherichia coli XL-1 blue	XL-1 Blue	Purchased from Addgene

845

846 **Supplemental Table S2. A list of plasmids used in this study.**

Plasmid name	**Description**	**Comments**	**Source**
pDM4	a CmR and oriV^{R6K}-containing suicide vector	Used as a backbone to construct plasmids for gene deletions in *Vibrio*	(O'Toole et al, 1996)
pDM4:*vprh*	pDM4 containing 1 kb upstream and 1 kb downstream of *vprh* in its MCS	Used to delete *vprh* in *V. proteolyticus*	(Ray et al., 2016)
pDM4:*hns1*	pDM4 containing 1 kb upstream and 1 kb downstream of *hns1* in its MCS	Used to delete *hns1* in *V. proteolyticus*	This study
pDM4:*tssG1*	pDM4 containing 1 kb upstream and 1 kb downstream of *tssG1* in its MCS	Used to delete *tssG1* in *V. proteolyticus*	(Ray et al., 2017)
pDM4:*tssL3*	pDM4 containing 1 kb upstream and 1 kb downstream of *tssL3* in	Used to delete *tssL3* in *V. proteolyticus*	This study

	its MCS		
pDM4:*tie1*	pDM4 containing 1 kb upstream and 1 kb downstream of the region corresponding to nucleotides 485-584 of *tie1* in its MCS	Used to delete a 100 bp region and inactivate *tie1* in *V. proteolyticus*	This study
pDM4:*tie2*	pDM4 containing 1 kb upstream and 1 kb downstream of *tie2* in its MCS	Used to delete *tie2* in *V. proteolyticus*	This study
pBAD/Myc-His^{Kan}	pBR322 ori-containing plasmid harboring a Kan^{R} cassette, araC, and an MCS following a P*bad* promoter	Used as a backbone to construct plasmids for arabinose-inducible gene expression	(Salomon et al., 2013)
pTssL3	pBAD/Myc-His^{Kan} containing the *tssL3* ORF in its MCS, in frame with a C-terminal Myc-His tag	Used for arabinose-inducible expression of TssL3	This study
pAts3	pBAD/Myc-His^{Kan} containing the *ats3* ORF in its MCS, not fused to a C-terminal tag	Used for arabinose-inducible expression of Ats3	This study
pTie1	pBAD/Myc-His^{Kan} containing the *tie1* ORF in its MCS, not fused to a C-terminal tag	Used for arabinose-inducible expression of Tie1	This study
pTie2	pBAD/Myc-His^{Kan} containing the *tie2* ORF in its MCS, not fused to	Used for arabinose-inducible expression of Tie2	This study

	a C-terminal tag		
pTie1-2	pBAD/Myc-His^{Kan} containing the ORFs of *tie1* and *tie2* in its MCS, not fused to a C-terminal tag	Used for arabinose-inducible expression of Tie1 and Tie2, together	This study
pBAD33.1	p15A ori-containing plasmid carrying a CmR gene, araC, and an MCS following a Pbad promoter.	Used for selection in competition assay	Purchased from Addgene; (Chung and Raetz, 2010)

847

848 **Supplemental Table S3. A list of primers used in this study.**

Primer name	**Sequence (5'-3')**	**Description**
VprHNS1_UP_F_ SacI	CAGCGAGCTCAAGACACTGGA CACGGTAG	Used to amplify 1 kb upstream of *hns1* to construct pDM4:*hns1*
VprHNS1_UP_R_ BamH	CAACGGATCCGACCATTCCTAT GAATTTAATAAAGTC	
VprHNS1_DN_F_ BamHI	CACCGGATCCTCGTAAGATTGG TTTAAAAAAGG	Used to amplify 1 kb downstream of *hns1* to construct pDM4:*hns1*
VprHNS1_DN_R_ SalI	CAACGTCGACCTATCGTTACCT GTGCAAC	
VprTssL3_UP_F_ SpeI	CACCACTAGTTGAAGACAGCC GTTTGCG	Used to amplify 1 kb upstream of *tssL3* to construct pDM4:*tssL3*
VprTssL3_UP_R_ HindIII	CAACAAGCTTAACTACCTACCT GATCAC	
VprTssl3_DN_F_ HindIII	CAGGAAGCTTTATGATCAAAAA AATTCTTG	Used to amplify 1 kb downstream of *tssL3* to construct pDM4:*tssL3*
VprTssL3_DN_R_ SphI	CAACGCATGCCCGGTTTTCACG CCCGATG	
VPR_ Tie1	CAAAGAGCTCGCGCAGACTTA	Used to amplify 1 kb

_SacI_UP_F	CGTTAAG	upstream of nucleotide 455 in *tie1* to construct pDM4:*tie1*
VPR_ Tie1 _XbaI_Up_R	CACCTCTAGATTTTGTAGAATC GTTCGCCCTGG	
VPR_ Tie1 _XbaI_DN_F	CACCTCTAGATGAGCTGGGCAT CAAGGCTGG	Used to amplify 1 kb downstream of nucleotide 584 in *tie1* to construct pDM4:*tie1*
VPR_Tie1 _SalI_DN_R	CAAAGTCGACTTTGCAAATTTT GCAGCAAACG	
VPR_Tie2_UP_F_ SacI	CATTGAGCTCACGGCCGGTGA ATTTAACG	Used to amplify 1 kb upstream of *tie2* to construct pDM4:*tie2*
VPR_Tie2_UP_R _HindIII	CAACAAGCTTAGGCCTTTCCTT TTTATTAACGTG	
VPR_Tie2_DN_F _HindIII	CACGAAGCTTTCCTTGCCAACA TAGCGG	Used to amplify 1 kb downstream of *tie2* to construct pDM4:*tie2*
VPR_Tie2_DN_R _SalI	CAGCGTCGACAATCTATAACAC TCACCG	
tssL3_F_pBADfix	GCTAACAGGAGGAATTAACCAT GGCAGGACTTTTTAACG	Used to amplify *tssL3* to construct pTssL3
tssL3_R_pBADfix	TTTTGTTCGGGCCCAAGCTTTT TCTGCGCTCTTCTTATCG	
Tie1_F_pBADfix	GCTAACAGGAGGAATTAACCAT GATAAATGATTTACAAAATGCC	Used to amplify *tie1* to construct pTie1and pTie1-2
Tie1_R_pBADfix	TTTTGTTCGGGCCCAAGCTTGA ATGTGCTCAGAATGTCCTGC	Used to amplify *tie1* to construct pTie1
Tie2_F_pBADfix	TTTTGTTCGGGCCCAAGCTTTC ACGCGGCTTCCGGGTGTG	Used to amplify *tie2* to construct pTie2
Tie1_Tie2_R_pBA Dfix	TTTTGTTCGGGCCCAAGCTTCG CGGCTTCCGGGTGTGGAGGCA GTAC	Used to amplify *tie2* to construct pTie2 and pTie1-2
Ats3_F_pBADfix	GCTAACAGGAGGAATTAACCAT GGAAAGAAAATCTATAACACTC	Used to amplify *Ats3* to construct pAts3
Ats3_R_pBADfix	TTTTGTTCGGGCCCAAGCTTTT AGCGCTGATAGCGTTTG	

Resource availability:

Lead Contact:

Further information and requests for resources and reagents should be directed to and will be fulfilled by the lead contact, Motti Gerlic (mgerlic@tauex.tau.ac.il).

Materials availability

Materials are available from the authors upon reasonable request.

Data and code availability

Data are, available from the authors upon reasonable request. This study did not generate new codes.

Supplemental information

Supplemental Figures

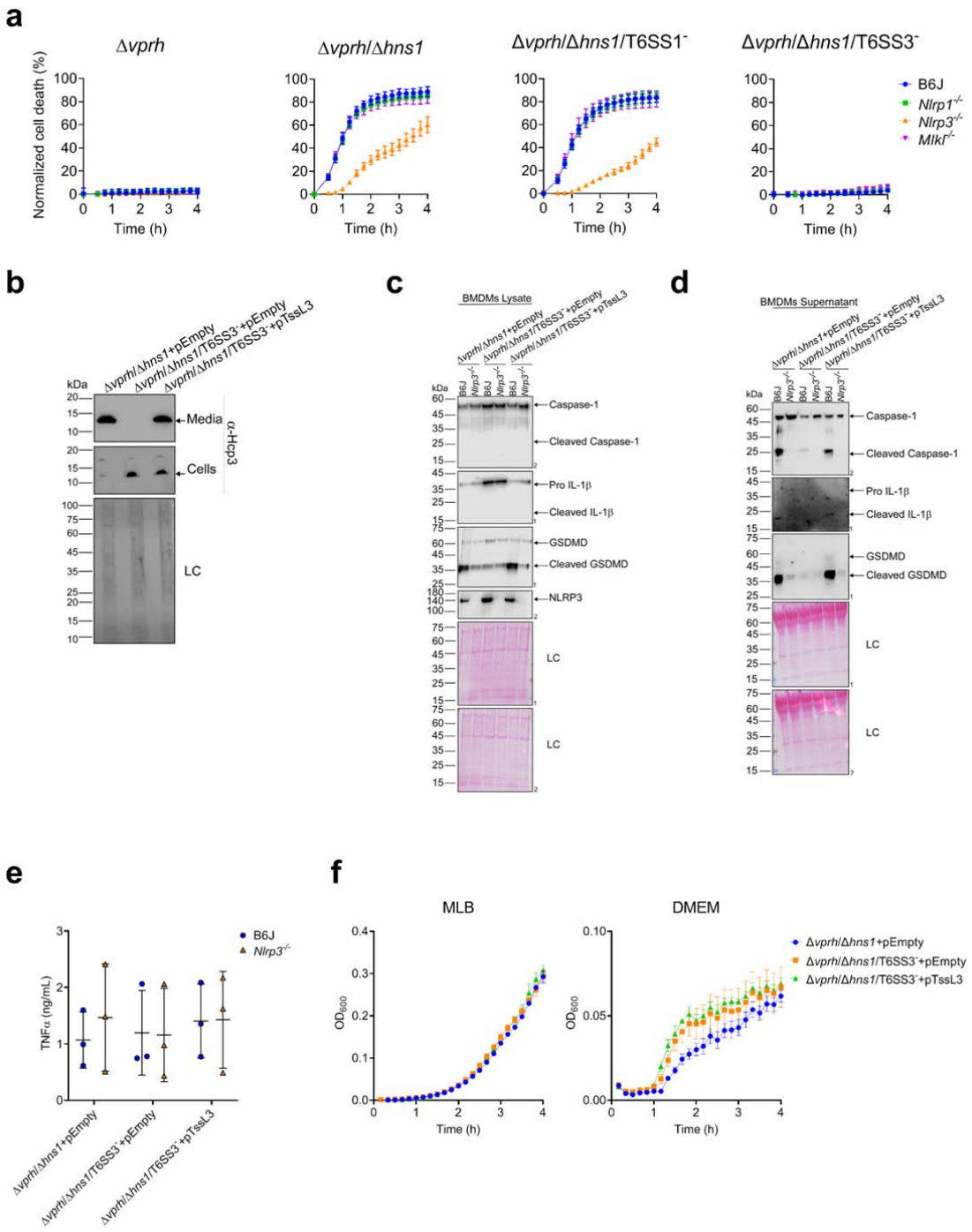

Supplemental Figure 1 (Related to Figure 3): T6SS3 activates the NLRP3 inflammasome in BMDMs

(a) PI uptake was assessed using real-time microscopy (IncucyteZOOM). The data are another depiction of the results shown in the experiment described in main Figure 3a. **(b)** The expression (cells) and secretion (media) of VgrG1 and Hcp3 from *V. proteolyticus* strains were detected by immunoblotting using specific antibodies. Loading control (LC) is shown for total protein lysate. An arrow denotes the expected band size of Hcp3. **(c-d)** NLRP3, Caspase-1, GSDMD, and IL-1β were detected in BMDM lysates (c) and supernatants (d) from experiments described in main Figure 3e-f by immunoblotting (the number on the right side of each blot denotes the blot number). **(e)** Cell supernatants from experiments described in main Figure 3e-f were collected 3 hours post infection. TNFα secretion was measured using a commercial ELISA kit. **(f)** Growth of *V. proteolyticus* strains in MLB or DMEM media supplemented with 0.05% arabinose at 30°C, measured as absorbance at 600 nm (OD_{600}). The data shown in (a-b, f) and (c-d) are a representative experiment out of n≥3 and two independent experiments, respectively. Statistical comparisons in (e) were performed using RM two-way ANOVA, followed by Turkey's multiple comparison test. The results are shown as the mean ± SD of 3 independent experiments; significant differences were considered as $P<0.05$.

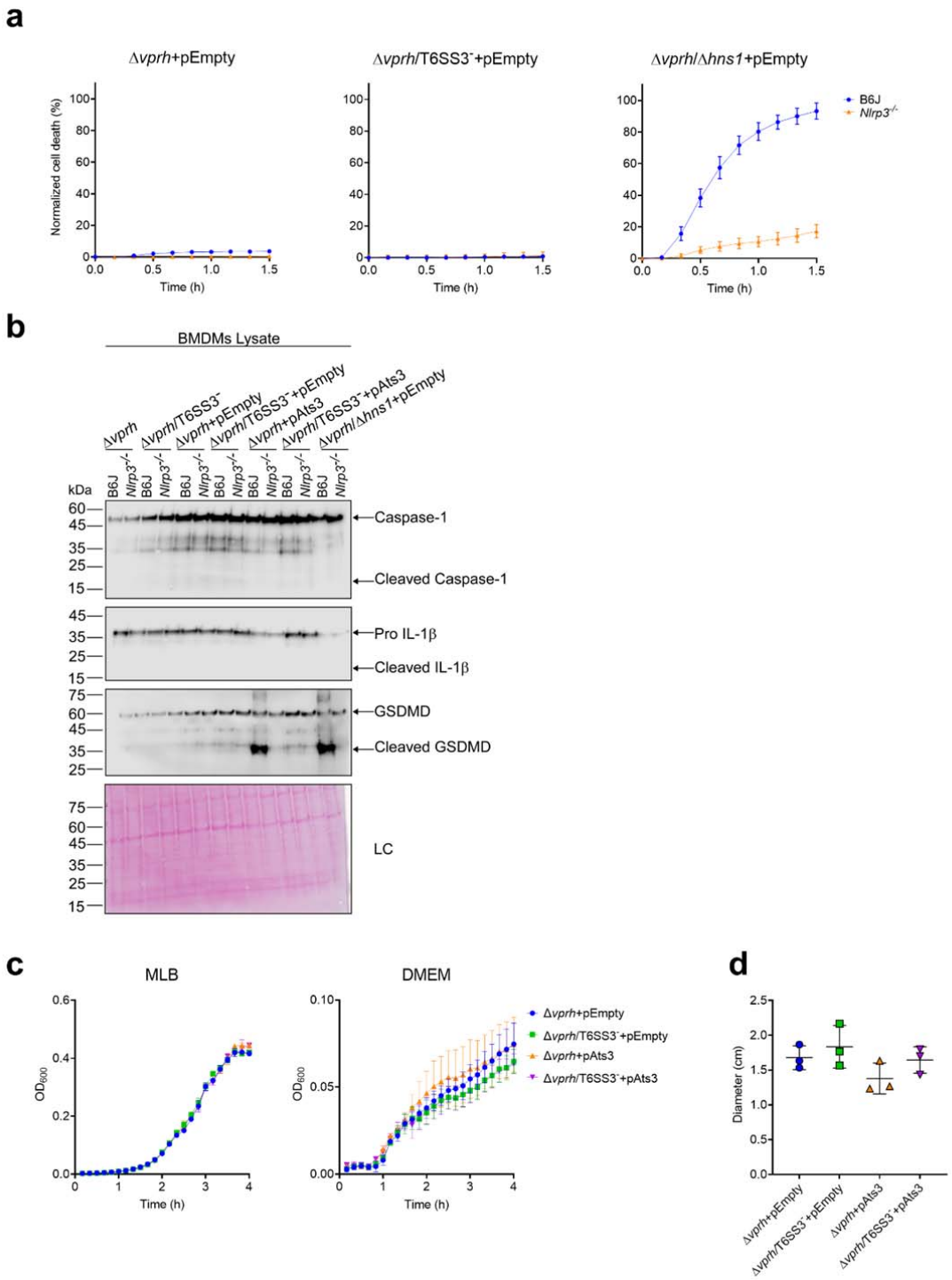

888

889 **Supplemental Figure 2 (Related to Figure 5): Activation of T6SS3 by Ats3 is**
890 **sufficient to induce the NLRP3 inflammasome**

891 **(a)** PI uptake was assessed using real-time microscopy (IncucyteZOOM). The data
892 are another depiction of the results shown in the experiment described in main
893 Figure 5d-g. **(b)** NLRP3, Caspase-1, GSDMD, and IL-1β were detected in BMDM

lysates by immunoblotting. Arrows denote the expected band size. The samples were taken from the experiment described in main Figure 5d-g. **(c)** Growth of *V. proteolyticus* strains, used in main Figure 5, in MLB or DMEM media supplemented with 0.05% arabinose at 30°C, measured as absorbance at 600 nm (OD_{600}). **(d)** Swimming motility of *V. proteolyticus* strains, measured as migration of a soft-agar plate supplemented with 0.1% arabinose after overnight incubation at 30°C. The data are shown as the mean ± SD of 3 biological repeats. Statistical comparison was preformed using RM one-way ANOVA, follow by Turkey's multiple comparison test.

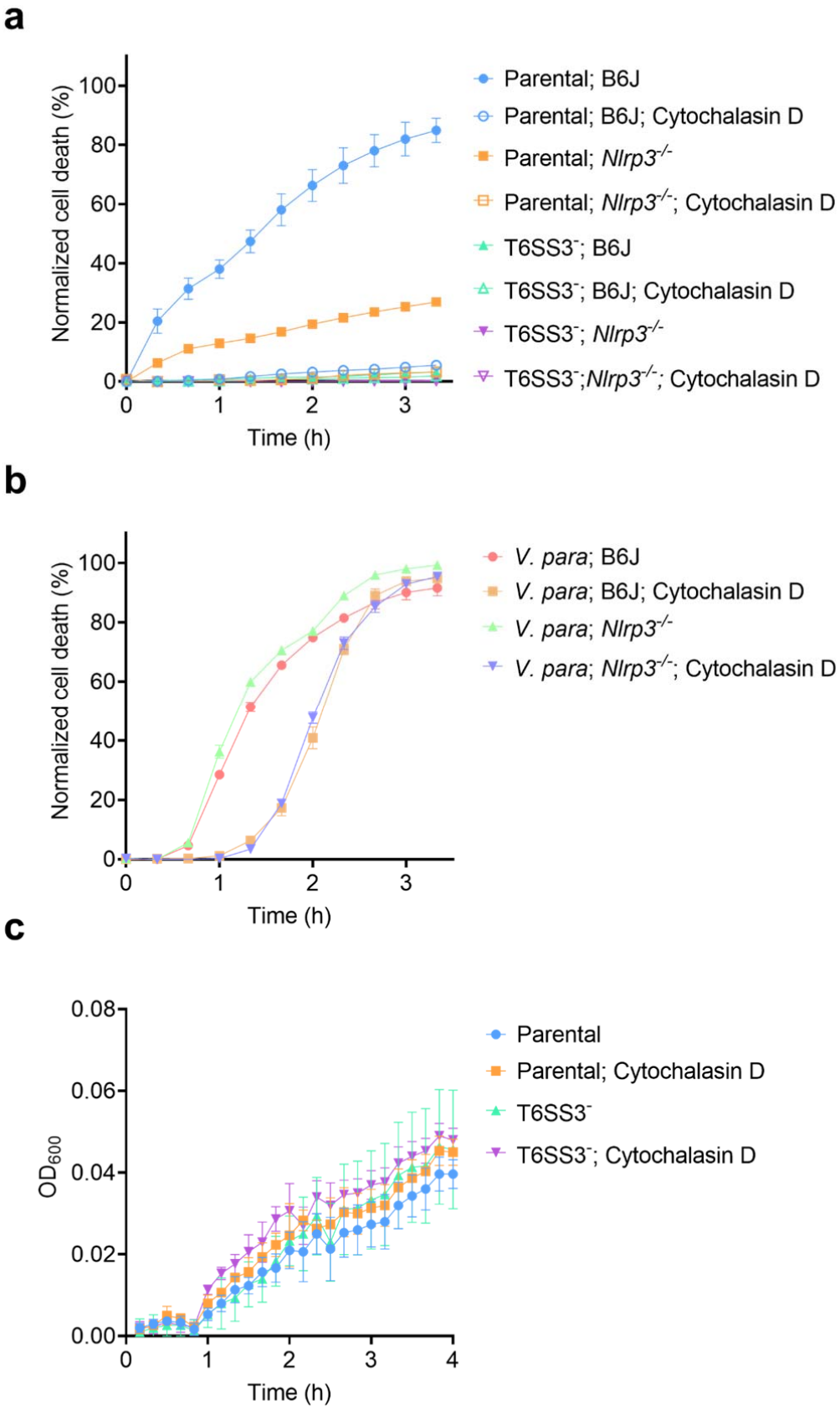

902

Supplemental Figure 3 (Related to Figure 6): *V. proteolyticus* T6SS3 activity requires phagocytosis

(a-b) Approximately 3.5*10^4 wild-type and *Nlrp3*$^{-/-}$ BMDMs were seeded into 96-well plates in 6 replicates and were primed using LPS (100 ng/mL) for 3 hours prior to infection with *V. proteolyticus* strains at MOI 5. **(a-b)** PI uptake was assessed using real-time microscopy (IncucyteZOOM) and then graphed as the AUC of the percentage of PI-positive cells normalized to the number of cells in the wells. Parental, V. proteolyticus Δ*vprh*+pAts3; *V. para*, *V. parahaemolyticus* RIMD 2210633 Δ*tdhAS* derivative. **(c)** Growth of *V. proteolyticus* strains used in main Figure 6a-e in DMEM media at 37°C, measured as absorbance at 600 nm (OD_{600}). Arabinose (0.05% w/v) was added to induce expression from the plasmid. Where indicated, 5 µM cytochalasin D were added to cells 45 minutes prior infection to inhibit phagocytosis. The data in (a-c) are shown as the mean ± SD, and are a representative experiment out of n=3 independent experiments.

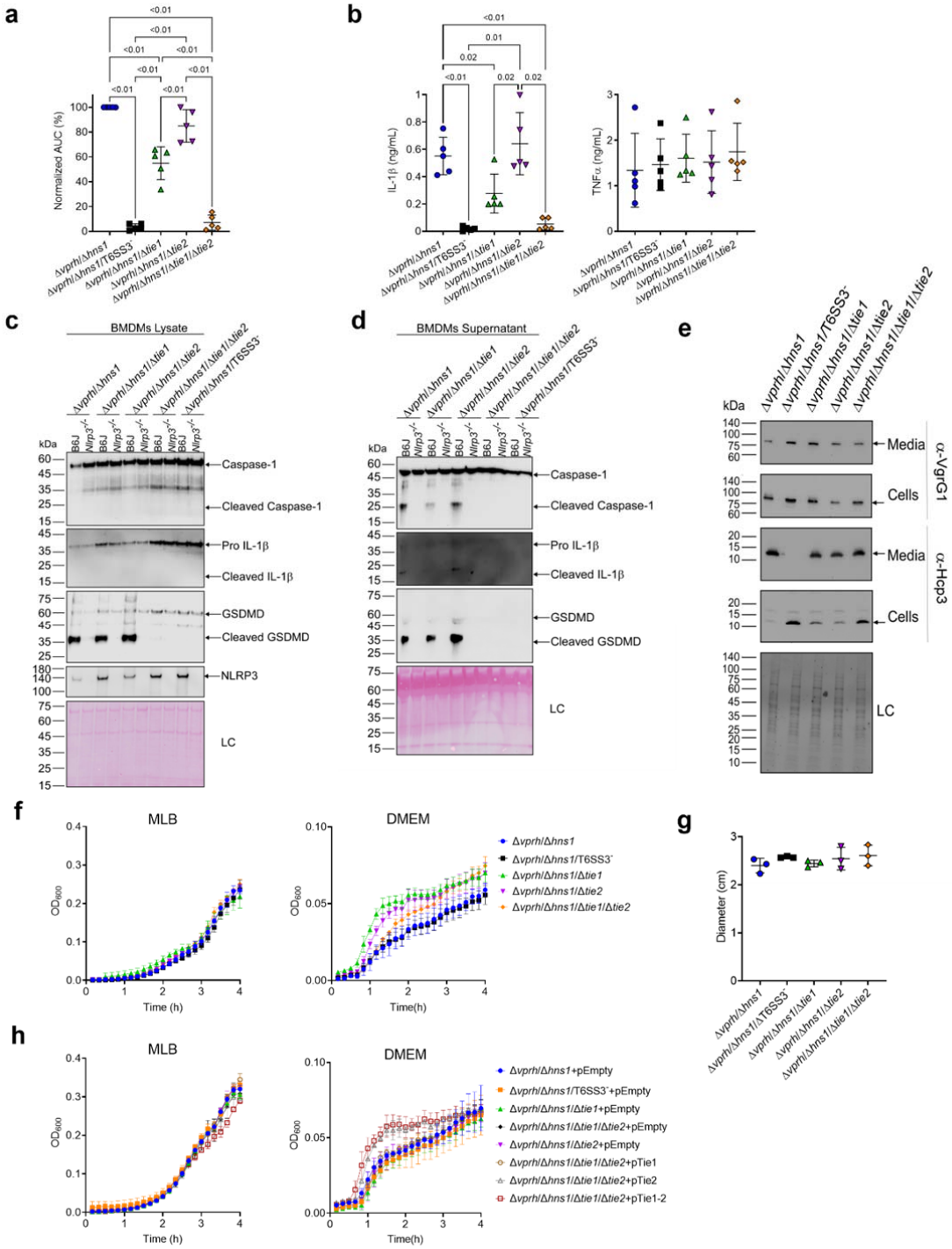

Supplemental Figure 4 (Related to Figure 7): Two T6SS3 effectors are necessary and sufficient to induce pyroptotic cell death

(a-d) Approximately 3.5*10^4 wild-type and *Nlrp3*$^{-/-}$ BMDMs were seeded into 96-well plates in 6 replicates and were primed using LPS (100 ng/mL) for 3 hours prior to infection with *V. proteolyticus* strains at MOI 5. (a) PI uptake was assessed using

real-time microscopy (IncucyteZOOM) and then graphed as the AUC of the percentage of PI-positive cells normalized to the number of cells in the wells. (b) Cell supernatants from experiments described in (a) were collected 3 hours post infection. IL-1β and TNFα secretion were measured using commercial ELISA kits. (c-d) NLRP3, Caspase-1, GSDMD, and IL-1β were detected in BMDM lysates (c) and supernatants (d) by immunoblotting. Arrows denote the expected band size. **(e)** The expression (cells) and secretion (media) of VgrG1 and Hcp3 from *V. proteolyticus* strains were detected by immunoblotting using specific antibodies. Loading control (LC) is shown for total protein lysate. **(f-h)** Growth of *V. proteolyticus* strains, used in (a-d) and in main Figure 7c-g, in MLB or DMEM media (in h, 0.05% arabinose was added at t=0 h to induce expression from the plasmid) at 30°C, measured as absorbance at 600 nm (OD_{600}). **(g)** Motility of *V. proteolyticus* used in (a-d). Swimming motility of *V. proteolyticus* strains, measured as migration on a soft-agar plate after overnight incubation at 30ºC. Statistical comparisons in (a-b) and (g) were performed using RM one-way ANOVA, followed by Dunnett's multiple comparison test. The results are shown as the mean ± SD of 3 independent experiments; a significant difference was considered as $P<0.05$. The results in (c-h) are of a representative experiment out of n≥2 independent experiments with similar results.

References

Aubert, D.F., Xu, H., Yang, J., Shi, X., Gao, W., Li, L., Bisaro, F., Chen, S., Valvano, M.A., and Shao, F. (2016). A Burkholderia Type VI Effector Deamidates Rho GTPases to Activate the Pyrin Inflammasome and Trigger Inflammation. Cell Host Microbe *19*, 664–674.

Baker-Austin, C., Oliver, J.D., Alam, M., Ali, A., Waldor, M.K., Qadri, F., and Martinez-Urtaza, J. (2018). Vibrio spp. infections. Nat. Rev. Dis. Prim. *4*, 8.

Bauernfried, S., Scherr, M.J., Pichlmair, A., Duderstadt, K.E., and Hornung, V. (2021). Human NLRP1 is a sensor for double-stranded RNA. Science (80-.). *371*, eabd0811.

Bensadoun, A., and Weinstein, D. (1976). Assay of proteins in the presence of interfering materials. Anal. Biochem. *70*, 241–250.

Bingle, L.E., Bailey, C.M., and Pallen, M.J. (2008). Type VI secretion: a beginner's guide. Curr. Opin. Microbiol. *11*, 3–8.

Bowden, T.J., Bricknell, I.R., and Preziosi, B.M. (2018). Comparative pathogenicity of Vibrio spp., Photobacterium damselae ssp. damselae and five isolates of Aeromonas salmonicida ssp. achromogenes in juvenile Atlantic halibut (Hippoglossus hippoglossus). J. Fish Dis. *41*, 79–86.

Boyer, F., Fichant, G., Berthod, J., Vandenbrouck, Y., and Attree, I. (2009). Dissecting the bacterial type VI secretion system by a genome wide in silico analysis: What can be learned from available microbial genomic resources? BMC Genomics *12*, 104.

Bröms, J.E., Sjöstedt, A., and Lavander, M. (2010). The role of the Francisella tularensis pathogenicity island in type VI secretion, intracellular survival, and modulation of host cell signaling. Front. Microbiol. *1*, 1–17.

969 Brown, S.S., and Spudich, J.A. (1979). Cytochalasin inhibits the rate of elongation of
970 actin filament fragments. J. Cell Biol. *83*, 657–662.
971 Bruto, M., James, A., Petton, B., Labreuche, Y., Chenivesse, S., Alunno-Bruscia, M.,
972 Polz, M.F., and Le Roux, F. (2017). Vibrio crassostreae, a benign oyster colonizer
973 turned into a pathogen after plasmid acquisition. ISME J. *11*, 1043–1052.
974 Burdette, D.L., Yarbrough, M.L., Orvedahl, A., Gilpin, C.J., and Orth, K. (2008).
975 Vibrio parahaemolyticus orchestrates a multifaceted host cell infection by induction
976 of autophagy, cell rounding, and then cell lysis. Proc. Natl. Acad. Sci. U. S. A. *105*,
977 12497–12502.
978 Cervino, J.M., Thompson, F.L., Gomez-Gil, B., Lorence, E.A., Goreau, T.J., Hayes,
979 R.L., Winiarski-Cervino, K.B., Smith, G.W., Hughen, K., and Bartels, E. (2008). The
980 Vibrio core group induces yellow band disease in Caribbean and Indo-Pacific reef-
981 building corals. J. Appl. Microbiol. *105*, 1658–1671.
982 Chen, H., Yang, D., Han, F., Tan, J., Zhang, L., Xiao, J., Zhang, Y., and Liu, Q.
983 (2017). The Bacterial T6SS Effector EvpP Prevents NLRP3 Inflammasome
984 Activation by Inhibiting the Ca 2+ -Dependent MAPK-Jnk Pathway. Cell Host
985 Microbe *21*, 47–58.
986 Chu, B., Yao, F., Cheng, C., Wu, Y., Mei, Y., Li, X., Liu, Y., Wang, P., Hou, L., and
987 Zou, X. (2014). The potential role of As-sumo-1 in the embryonic diapause process
988 and early embryo development of Artemia sinica. PLoS One *9*, e85343.
989 Chung, H.S., and Raetz, C.R.H. (2010). Interchangeable domains in the Kdo
990 transferases of escherichia coli and haemophilus influenzae. Biochemistry *49*, 4126–
991 4137.
992 Church, L.D., Cook, G.P., and McDermott, M.F. (2008). Primer: inflammasomes and
993 interleukin 1β in inflammatory disorders. Nat. Clin. Pract. Rheumatol. *4*, 34–42.

994 Clemens, D.L., Lee, B.Y., and Horwitz, M.A. (2018). The Francisella Type VI
995 secretion system. Front. Cell. Infect. Microbiol. *8*, 1–20.
996 Cohen, H., Baram, N., Edry-Botzer, L., Munitz, A., Salomon, D., and Gerlic, M.
997 (2020). Vibrio pore-forming leukocidin activates pyroptotic cell death via the NLRP3
998 inflammasome. Emerg. Microbes Infect. *9*, 278–290.
999 Conos, S.A., Chen, K.W., De Nardo, D., Hara, H., Whitehead, L., Núñez, G.,
1000 Masters, S.L., Murphy, J.M., Schroder, K., Vaux, D.L., et al. (2017). Active MLKL
1001 triggers the NLRP3 inflammasome in a cell-intrinsic manner. Proc. Natl. Acad. Sci.
1002 U. S. A. E961–E969.
1003 Dar, Y., Salomon, D., and Bosis, E. (2018). The Antibacterial and Anti-Eukaryotic
1004 Type VI Secretion System MIX-Effector Repertoire in Vibrionaceae. Mar. Drugs *16*,
1005 433.
1006 Dinarello, C.A. (2018). Overview of the IL-1 family in innate inflammation and
1007 acquired immunity. Immunol. Rev. *281*, 8–27.
1008 Dorman, C.J. (2004). H-NS: A universal regulator for a dynamic genome. Nat. Rev.
1009 Microbiol. *2*, 391–400.
1010 Flanagan, M.D., and Lin, S. (1980). Cytochalasins block actin filament elongation by
1011 binding to high affinity sites associated with F-actin. J. Biol. Chem. *255*, 835–838.
1012 Franklin, B.S., Bossaller, L., De Nardo, D., Ratter, J.M., Stutz, A., Engels, G.,
1013 Brenker, C., Nordhoff, M., Mirandola, S.R., Al-Amoudi, A., et al. (2014). The adaptor
1014 ASC has extracellular and “prionoid” activities that propagate inflammation. Nat.
1015 Immunol. *15*, 727–737.
1016 Frans, I., Michiels, C.W., Bossier, P., Willems, K.A., Lievens, B., and Rediers, H.
1017 (2011). Vibrio anguillarum as a fish pathogen: Virulence factors, diagnosis and
1018 prevention. J. Fish Dis. *34*, 643–661.

Geller, A.M., Pollin, I., Zlotkin, D., Danov, A., Nachmias, N., Andreopoulos, W.B., Shemesh, K., and Levy, A. (2021). The extracellular contractile injection system is enriched in environmental microbes and associates with numerous toxins. Nat. Commun. *12*, 1–15.

Gibson, D.G., Young, L., Chuang, R.Y., Venter, J.C., Hutchison, C.A., and Smith, H.O. (2009). Enzymatic assembly of DNA molecules up to several hundred kilobases. Nat. Methods *6*, 343–345.

Hachani, A., Wood, T.E., and Filloux, A. (2016). Type VI secretion and anti-host effectors. Curr. Opin. Microbiol. *29*, 81–93.

Isherwood, B., Timpson, P., Mcghee, E.J., Anderson, K.I., Canel, M., Serrels, A., Brunton, V.G., and Carragher, N.O. (2011). Live cell in vitro and in vivo imaging applications: Accelerating drug discovery. Pharmaceutics *3*, 141–170.

Jiang, F., Waterfield, N.R., Yang, J., Yang, G., and Jin, Q. (2014). A Pseudomonas aeruginosa type VI secretion phospholipase D effector targets both prokaryotic and eukaryotic cells. Cell Host Microbe *15*, 600–610.

Jiang, S., Zhou, Z., Sun, Y., Zhang, T., and Sun, L. (2020). Coral gasdermin triggers pyroptosis. Sci. Immunol. *5*, eabd2591.

Lamkanfi, M., and Dixit, V.M. (2014). Mechanisms and functions of inflammasomes. Cell *157*, 1013–1022.

Lawlor, K.E., Khan, N., Mildenhall, A., Gerlic, M., Croker, B.A., D'Cruz, A.A., Hall, C., Kaur Spall, S., Anderton, H., Masters, S.L., et al. (2015). RIPK3 promotes cell death and NLRP3 inflammasome activation in the absence of MLKL. Nat. Commun. *18*, 6282.

Li, P., Kinch, L.N., Ray, A., Dalia, A.B., Cong, Q., Nunan, L.M., Camilli, A., Grishin, N. V., Salomon, D., and Orth, K. (2017). Acute hepatopancreatic necrosis disease-

causing Vibrio parahaemolyticus strains maintain an antibacterial type VI secretion system with versatile effector repertoires. Appl. Environ. Microbiol. *83*, 1–17.

Lieberman, J., Wu, H., and Kagan, J.C. (2019). Gasdermin D activity in inflammation and host defense. Sci. Immunol. *4*, eaav1447.

Liu, X., Zhang, Z., Ruan, J., Pan, Y., Magupalli, V.G., Wu, H., and Lieberman, J. (2016). Inflammasome-activated gasdermin D causes pyroptosis by forming membrane pores. Nature *535*, 153–158.

Lu, S., Wang, J., Chitsaz, F., Derbyshire, M.K., Geer, R.C., Gonzales, N.R., Gwadz, M., Hurwitz, D.I., Marchler, G.H., Song, J.S., et al. (2020). CDD/SPARCLE: The conserved domain database in 2020. Nucleic Acids Res. *48*, D265–D268.

Luchetti, G., Roncaioli, J.L., Chavez, R.A., Schubert, A.F., Kofoed, E.M., Reja, R., Cheung, T.K., Liang, Y., Webster, J.D., Lehoux, I., et al. (2021). Shigella ubiquitin ligase IpaH7.8 targets gasdermin D for degradation to prevent pyroptosis and enable infection. Cell Host Microbe *29*, 1521-1530.e10.

Ma, A.T., McAuley, S., Pukatzki, S., and Mekalanos, J.J. (2009). Translocation of a Vibrio cholerae Type VI Secretion Effector Requires Bacterial Endocytosis by Host Cells. Cell Host Microbe *5*, 234–243.

Man, S.M., Karki, R., and Kanneganti, T.D. (2017). Molecular mechanisms and functions of pyroptosis, inflammatory caspases and inflammasomes in infectious diseases. Immunol. Rev. 61–75.

Miller, K.A., Tomberlin, K.F., and Dziejman, M. (2019). Vibrio variations on a type three theme. Curr. Opin. Microbiol. *47*, 66–73.

Monjarás Feria, J., and Valvano, M.A. (2020). An Overview of Anti-Eukaryotic T6SS Effectors. Front. Cell. Infect. Microbiol. *10*, 584751.

Mougous, J.D., Cuff, M.E., Raunser, S., Shen, A., Zhou, M., Gifford, C.A., Goodman,

A.L., Joachimiak, G., Ordoñez, C.L., Lory, S., et al. (2006). A virulence locus of Pseudomonas aeruginosa encodes a protein secretion apparatus. Science (80-.). *312*, 1526–1530.

O'Toole, R., Milton, D.L., and Wolf-Watz, H. (1996). Chemotactic motility is required for invasion of the host by the fish pathogen Vibrio anguillarum. Mol. Microbiol. *19*, 625–637.

Park, K.S., Ono, T., Rokuda, M., Jang, M.H., Iida, T., and Honda, T. (2004). Cytotoxicity and Enterotoxicity of the Thermostable Direct Hemolysin-Deletion Mutants of Vibrio parahaemolyticus. Microbiol. Immunol. *48*, 313–318.

Potter, S.C., Luciani, A., Eddy, S.R., Park, Y., Lopez, R., and Finn, R.D. (2018). HMMER web server: 2018 update. Nucleic Acids Res. *46*, W200–W204.

Proell, M., Gerlic, M., Mace, P.D., Reed, J.C., and Riedl, S.J. (2013). The CARD plays a critical role in ASC foci formation and inflammasome signalling. Biochem. J. *449*, 613–621.

Pukatzki, S., Ma, A.T., Sturtevant, D., Krastins, B., Sarracino, D., Nelson, W.C., Heidelberg, J.F., and Mekalanos, J.J. (2006). Identification of a conserved bacterial protein secretion system in Vibrio cholerae using the Dictyostelium host model system. Proc. Natl. Acad. Sci. U. S. A. *103*, 1528–1533.

Pukatzki, S., Ma, A.T., Revel, A.T., Sturtevant, D., and Mekalanos, J.J. (2007). Type VI secretion system translocates a phage tail spike-like protein into target cells where it cross-links actin. Proc. Natl. Acad. Sci. U. S. A. *104*, 15508–15513.

Ray, A., Kinch, L.N., de Souza Santos, M., Grishin, N. V., Orth, K., and Salomon, D. (2016). Proteomics Analysis Reveals Previously Uncharacterized Virulence Factors in Vibrio proteolyticus. MBio *7*, e01077-16.

Ray, A., Schwartz, N., Souza Santos, M., Zhang, J., Orth, K., and Salomon, D.

(2017). Type VI secretion system MIX-effectors carry both antibacterial and anti-eukaryotic activities. EMBO Rep. *18*, 1978–1990.

Rosales-Reyes, R., Skeldon, A.M., Aubert, D.F., and Valvano, M.A. (2012). The Type VI secretion system of Burkholderia cenocepacia affects multiple Rho family GTPases disrupting the actin cytoskeleton and the assembly of NADPH oxidase complex in macrophages. Cell. Microbiol. *14*, 255–273.

Roux, F. Le, Wegner, K.M., Baker-Austin, C., Vezzulli, L., Osorio, C.R., Amaro, C., Ritchie, J.M., Defoirdt, T., Destoumieux-Garzón, D., Blokesch, M., et al. (2015). The emergence of Vibrio pathogens in Europe: ecology, evolution, and pathogenesis (Paris, 11–12th March 2015). Front. Microbiol. *6*, 830.

Sagulenko, V., Vitak, N., Vajjhala, P.R., Vince, J.E., and Stacey, K.J. (2018). Caspase-1 Is an Apical Caspase Leading to Caspase-3 Cleavage in the AIM2 Inflammasome Response, Independent of Caspase-8. J. Mol. Biol. *430*, 238–247.

Salomon, D., Gonzalez, H., Updegraff, B.L., and Orth, K. (2013). Vibrio parahaemolyticus Type VI Secretion System 1 Is Activated in Marine Conditions to Target Bacteria, and Is Differentially Regulated from System 2. PLoS One *8*, e61086.

Salomon, D., Klimko, J.A., and Orth, K. (2014). H-NS regulates the Vibrio parahaemolyticus type VI secretion system 1. Microbiology *160*, 1867–1873.

Salomon, D., Klimko, J.A., Trudgian, D.C., Kinch, L.N., Grishin, N. V., Mirzaei, H., and Orth, K. (2015). Type VI Secretion System Toxins Horizontally Shared between Marine Bacteria. PLOS Pathog. *11*, e1005128.

Sana, T.G., Baumann, C., Merdes, A., Soscia, C., Rattei, T., Hachani, A., Jones, C., Bennett, K.L., Filloux, A., Superti-Furga, G., et al. (2015). Internalization of Pseudomonas aeruginosa strain PAO1 into epithelial cells is promoted by interaction

of a T6SS effector with the microtubule network. MBio *6*, 1–11.

Schroder, K., and Tschopp, J. (2010). The Inflammasomes. Cell *140*, 821–832.

Shalom, G., Shaw, J.G., and Thomas, M.S. (2007). In vivo expression technology identifies a type VI secretion system locus in Burkholderia pseudomallei that is induced upon invasion of macrophages. Microbiology *153*, 2689–2699.

Shao, B.-Z., Xu, Z.-Q., Han, B.-Z., Su, D.-F., and Liu, C. (2015). NLRP3 inflammasome and its inhibitors: a review. Front. Pharmacol. *6*, 262.

Shi, J., Zhao, Y., Wang, K., Shi, X., Wang, Y., Huang, H., Zhuang, Y., Cai, T., Wang, F., and Shao, F. (2015). Cleavage of GSDMD by inflammatory caspases determines pyroptotic cell death. Nature *526*, 660–665.

Stephen F.Altschul, Warren Gish, Webb Miller, Eugene W.Myers, D.J.L. (1990). Basic local alignment search tool. J. Mol. Biol. *215*, 403–410.

Swanson, K. V., Deng, M., and Ting, J.P.-Y. (2019). The NLRP3 inflammasome: molecular activation and regulation to therapeutics. Nat. Rev. Immunol. *19*, 477–489.

Tran, H.R., Grebenc, D.W., Klein, T.A., Whitney, J.C., Whitney, J.C., and Degroote, M. (2021). Bacterial type VII secretion : An important player in host-microbe and microbe-microbe interactions. *115*, 478–489.

Trouplin, V., Boucherit, N., Gorvel, L., Conti, F., Mottola, G., and Ghigo, E. (2013). Bone marrow-derived macrophage production. J. Vis. Exp. e50966.

Tsuchiya, K., Nakajima, S., Hosojima, S., Thi Nguyen, D., Hattori, T., Manh Le, T., Hori, O., Mahib, M.R., Yamaguchi, Y., Miura, M., et al. (2019). Caspase-1 initiates apoptosis in the absence of gasdermin D. Nat. Commun. *10*, 2091.

Verschuere, L., Heang, H., Criel, G., Sorgeloos, P., and Verstraete, W. (2000). Selected bacterial strains protect Artemia spp. from the Pathogenic effects of Vibrio proteolyticus CW8T2. Appl. Environ. Microbiol. *66*, 1139–1146.

1144 Vezzulli, L., Grande, C., Reid, P.C., Hélaouët, P., Edwards, M., Höfle, M.G., Brettar,
1145 I., Colwell, R.R., and Pruzzo, C. (2016). Climate influence on Vibrio and associated
1146 human diseases during the past half-century in the coastal North Atlantic. Proc. Natl.
1147 Acad. Sci. U. S. A. *113*, E5062–E5071.
1148 Wallach, D., Kang, T.B., and Kovalenko, A. (2014). Concepts of tissue injury and cell
1149 death in inflammation: A historical perspective. Nat. Rev. Immunol. *14*, 51–59.
1150 Wang, X., Wang, Q., Xiao, J., Liu, Q., Wu, H., Xu, L., and Zhang, Y. (2009).
1151 Edwardsiella tarda T6SS component evpP is regulated by esrB and iron , and plays
1152 essential roles in the invasion of fish. Fish Shellfish Immunol. *27*, 469–477.
1153 Wen, H., Miao, E.A., and Ting, J.P.Y. (2013). Mechanisms of NOD-like receptor-
1154 associated inflammasome activation. Immunity *39*, 432–441.
1155 Whitney, J.C., Peterson, S.B., Kim, J., Pazos, M., Verster, A.J., Radey, M.C.,
1156 Kulasekara, H.D., Ching, M.Q., Bullen, N.P., Bryant, D., et al. (2017). A broadly
1157 distributed toxin family mediates contact-dependent antagonism between gram-
1158 positive bacteria. Elife *6*, 1–24.
1159 Zhou, B., and Abbott, D.W. (2021). Gasdermin E permits interleukin-1 beta release
1160 in distinct sublytic and pyroptotic phases. Cell Rep. *35*, 108998.
1161